Palaeogeography, Palaeoclimatology, Palaeoecology 677 (2025) 113190

Contents lists available at ScienceDirect

Palaeogeography, Palaeoclimatology, Palaeoecology

journal homepage: www.elsevier.com/locate/palaeo

Core-top constraints on the ecology and paleothermometry of planktic foraminifera in the Indian Ocean

Ryan H. Glaubke [a,*,1], Elisabeth L. Sikes [a], Natalie E. Umling [a,b], Katherine A. Allen [c], Matthew W. Schmidt [d]

[a] Department of Marine and Coastal Sciences, Rutgers University, New Brunswick, NJ, USA
[b] Department of Earth and Planetary Sciences, American Museum of Natural History, New York, NY, USA
[c] School of Earth and Climate Sciences, University of Maine, Orono, ME, USA
[d] Department of Ocean and Earth Sciences, Old Dominion University, Norfolk, VA, USA

ARTICLE INFO

Editor: Prof. M Elliot

Keywords:
Foraminifera
Mg/Ca
Core top
Indian Ocean
Calibration

ABSTRACT

The magnesium-to-calcium ratio (Mg/Ca) of fossil foraminifera is a widely used geochemical proxy for reconstructing past ocean temperatures. Culturing experiments have shown that, for some species, nonthermal influences like salinity and carbonate chemistry play a non-trivial role in the incorporation of Mg into foraminiferal calcite. Inclusion of these variables into Mg/Ca calibrations have provided a better fit to core top and sediment trap data in some recent studies, but the widespread covariation of potential control variables in the open ocean and the lack of multivariate calibrations for some species warrants additional work. Here, we assess Mg/Ca calibrations for four common species of planktic foraminifera from the Indian Ocean: *Globigerinoides ruber* (white; sensu lato), *Globigerina bulloides*, *Globorotalia inflata*, and *Globorotalia truncatulinoides* (sinistral). Using a newly assembled database of paired Mg/Ca-$\delta^{18}O$ observations from 115 Indian Ocean core tops, including 25 new observations from a 2018 cruise (CROCCA-2S), we build a multi-parameter environmental dataset informed by local constraints on each species' apparent calcification depth and growth season. We combine multivariate regression techniques with Bayesian factor analysis to develop several multivariate models and assess whether they improve model fit and performance over temperature-only equations. For *G. ruber*, the temperature-only model is the best empirical fit to our data ($Mg/Ca = exp.(0.086*(T - 25)) + 1.49$). Although we find a statistically significant relationship to seawater pH, its impact on estimated temperatures (± 0.65 °C per 0.1 pH unit) is smaller than the total uncertainty on the temperature-only model (±1.2 °C; 95 % CI). The Mg/Ca of *G. bulloides* is most reasonably described by a temperature-only model ($Mg/Ca = exp.(0.068*(T - 25)) + 1.51$). An apparent negative correlation between *G. bulloides* Mg/Ca and salinity is not consistent with prior culture and field studies, which have yielded only positive correlations (if any). This anomalous result is likely a byproduct of including core tops from the monsoon-sensitive Java/Sumatran coast. Finally, the Mg/Ca of subsurface-dwelling *G. inflata* and *G. truncatulinoides* fell within predicted ranges of some published calibrations, suggesting they might be effectively applied in this region. However, data for these two species were only available for cores from the southeast Indian Ocean where deep ocean mixing limits the dynamic range temperature, salinity, and other parameters across their habitat depth, preventing the creation of new, regionally robust calibrations. Overall, our work offers new calibrations for surface-dwelling species (*G. ruber* and *G. bulloides*) in the Indian Ocean and provides a framework for further refining multivariate controls on Mg/Ca of subsurface-dwelling species in the region.

1. Introduction

The upper ocean is a key component of the Earth-climate system, and constraining its thermal history is critical for clarifying the ocean's role in past global climate change (Lea, 2014). One of the most common methods for reconstructing past ocean temperatures is the analysis of the

* Corresponding author.
E-mail address: glaubke@arizona.edu (R.H. Glaubke).
[1] Now at Department of Geosciences, University of Arizona, Tucson, AZ, USA.

https://doi.org/10.1016/j.palaeo.2025.113190
Received 15 January 2025; Received in revised form 9 June 2025; Accepted 8 August 2025
Available online 11 August 2025

magnesium-to-calcium ratio (Mg/Ca) of fossil foraminifera preserved in marine sediments (e.g., Anand et al., 2003; Dekens et al., 2002; Lea et al., 1999; Nürnberg et al., 1996; Rosenthal et al., 2000). Planktic foraminifera primarily live in the upper water column where vertical gradients in hydrography (temperature and salinity), light, and food availability sort species into well-defined ecological niches (Schiebel and Hemleben, 2017). This sorting provides an opportunity to reconstruct temperatures from targeted depths in the uppermost water column (e.g., the mixed layer or sub-thermocline) or, by employing a multi-species approach, to reconstruct the thermal structure of the upper water column (Spero et al., 2003). The environmental conditions that set these ecological niches can vary, however, particularly in the subsurface where changes in the strength and depth of the thermocline can modify the living depth of subsurface-dwelling foraminiferal species (Cléroux et al., 2008; Hemleben et al., 1985; Romero et al., 2023). Local constraints on foraminiferal ecology are therefore an important predicate to refining the relationship between Mg/Ca and environmental conditions in the field, especially in regions where contemporary ecological surveys (e.g., from plankton tows) are not available.

The theoretical foundation of the Mg/Ca temperature proxy is rooted in the endothermic substitution of Mg for Ca in the calcite matrix of the foraminiferal shell (Navrotsky and Capobianco, 1987). Thermodynamic theory (Koziol and Newton, 1995), experiments with inorganic calcite (e.g., Oomori et al., 1987), and calibrations with cultured and fossil foraminifera (e.g., Anand et al., 2003; Dekens et al., 2002; Lea et al., 1999; Nürnberg et al., 1996; Rosenthal et al., 2000) each demonstrate that Mg/Ca increases exponentially with rising temperature. Early calibrations of foraminiferal Mg/Ca argued that temperature was the dominant control with an apparent sensitivity between ~8–10 % per °C (Anand et al., 2003; Dekens et al., 2002; Lea et al., 1999; Nürnberg et al., 1996; Rosenthal et al., 2000). However, culture experiments under carefully controlled environmental conditions have revealed that nonthermal influences play a significant role in determining foraminiferal Mg/Ca, with salinity (Lea et al., 1999; Hönisch et al., 2013) and carbonate chemistry (Russell et al., 2004; Evans et al., 2016) being the most cited examples. Some studies conclude that nonthermal parameters, rather than temperature, dominate the foraminiferal Mg/Ca signal (e.g., Arbuszewski et al., 2010; Ferguson et al., 2008). While reexaminations of the data and methods from these studies offer compelling alternative explanations for their findings (Hertzberg and Schmidt, 2013; Hoogakker et al., 2009), the results have nonetheless undermined the perception of the Mg/Ca proxy as a simple "paleothermometer", with a notable decline in the proxy's use over the last decade (Gray and Evans, 2019). The uncertainty in the fidelity of temperature-only Mg/Ca calibrations has led to the development of multivariate calibrations—mostly for surface-dwelling species—that account for nonthermal influences (e.g., Gray et al., 2018; Gray and Evans, 2019; Holland et al., 2020; Khider et al., 2015; Saenger and Evans, 2019; Tierney et al., 2019). While these calibrations typically provide a better fit to observations than temperature-only equations, this may come at the cost of a calibration's generalizability, a phenomenon known as overfitting (Saenger and Evans, 2019).

The development of field-based Mg/Ca calibrations therefore depends on two critical components: (1) estimates of the hydrographic conditions where calcification occurs, which relies on independent ecological constraints that account for spatial (living depth) and temporal variability (growing season); and (2) a better understanding of how nonthermal parameters influence Mg/Ca-based temperature estimates and whether these should be accounted for in down-core reconstructions. Here, we aim to constrain the ecology and ground-truth the Mg/Ca paleothermometer for four common species of planktic foraminifera in the Indian Ocean: *Globigerinoides ruber* (sensu lato; also referred to as *G. elongatus*), *Globigerina bulloides*, *Globorotalia inflata*, and *Globorotalia truncatulinoides* (sinistral coiling). Using a newly assembled database of paired stable oxygen isotope ($\delta^{18}O$) and Mg/Ca observations from 115 sediment core tops in the Indian Ocean, we estimate the apparent calcification depth (ACD) of each species and use temperature, salinity, and carbonate system parameters from those depths to develop temperature-only and multivariate Mg/Ca calibration models. We adopt a Bayesian approach to assess whether models with significant nonthermal influences sufficiently improve model fit and performance over temperature-only models (Holland et al., 2020). This method offers a robust framework for calibrating multivariate Mg/Ca models and systematically testing their skill over simpler models.

2. Methods

2.1. Data Compilation

Our calibrations are based on a newly compiled multi-species database of paired Mg/Ca-$\delta^{18}O$ measurements from Holocene-aged surface sediments across the Indian Ocean (Fig. 1 and Table S1). We focus our attention on the Indian Ocean because planktic foraminiferal paleoecology is relatively less well constrained here than in other global oceans, particularly for subsurface-dwelling species near the subtropical convergence. New analyses were conducted on 25 core tops from the south Indian Ocean collected as part of the Coring to Reconstruct Ocean Circulation and Carbon dioxide Across 2 Seas (CROCCA-2S) expedition in Boreal Fall 2018 (Table 1). These data were combined with published observations from the Arabian Sea (Dahl and Oppo, 2006), the Java/Sumatran coast (Mohtadi et al., 2011), and the Southern Ocean frontal region (Riveiros et al., 2016) to form a network of cores extending from 24°N - 49°S and from 51 to 5168 m depth. All CROCCA-2S core tops were dated using radiocarbon analysis on *G. inflata* at the Keck Carbon Cycle AMS facility at the University of California, Irvine. Final ages were calibrated against the Marine20 dataset (Heaton et al., 2020) using the latest version of the Calib software (v8.2) (Table S2). Four core tops that returned ages > ~6000 cal yrs BP were excluded from the analysis to yield a final dataset of 115 core tops.

Environmental data from overlying waters were sourced from the 2018 World Ocean Atlas (WOA18) database and the second version of the Global Ocean Data Analysis Project's gridded carbon climatology (GLODAP v2.2016b) (Lauvset et al., 2016). We opted to use these climatologies over in situ observations because data products incorporate multiple observational datasets collected over time, which better reflects the integrated environmental signal preserved in fossil foraminiferal populations. Both products are gridded at a 1° lateral resolution, although the vertical resolution of WOA18 (102 depth levels) is higher than GLODAP (57 depth levels). We linearly interpolated the GLODAP database to match the depth levels of WOA18. From each grid cell corresponding to a core location, we indexed monthly and mean annual depth profiles of temperature, salinity, silicate, and phosphate from WOA18, as well as mean annual profiles of dissolved inorganic carbon, alkalinity, pH, and calcite saturation from GLODAP (Fig. S1). In the few instances where data were unavailable, profiles were constructed by averaging available data from immediately adjacent grid cells. The ocean profile data that make up WOA18 are well distributed throughout the Indian Ocean and were almost always located within 100 km of our core sites. The casts underlying GLODAP are sparser in the region, with the nearest cast being on average 195 ± 117 km from our core sites.

2.2. Analytical techniques

We focus on our analysis on *G. ruber* (white; sensu lato; 250–355 μm), *G. bulloides* (250–355 μm), *G. inflata* (250–355 μm), and *G. truncatulinoides* (sinistral; 355–500 μm) given their prevalence in the CROCCA-2S core tops. During sampling, we avoided noticeably encrusted specimens given evidence suggesting they exhibit different shell chemistries, particularly for *G. inflata* and *G. truncatulinoides* (Jonkers et al., 2021; Rebotim et al., 2019; Reynolds et al., 2018).

Approximately 30–50 μg of foraminiferal tests was allocated for stable isotopic analyses. Samples were sonicated in methanol for 1–2 s

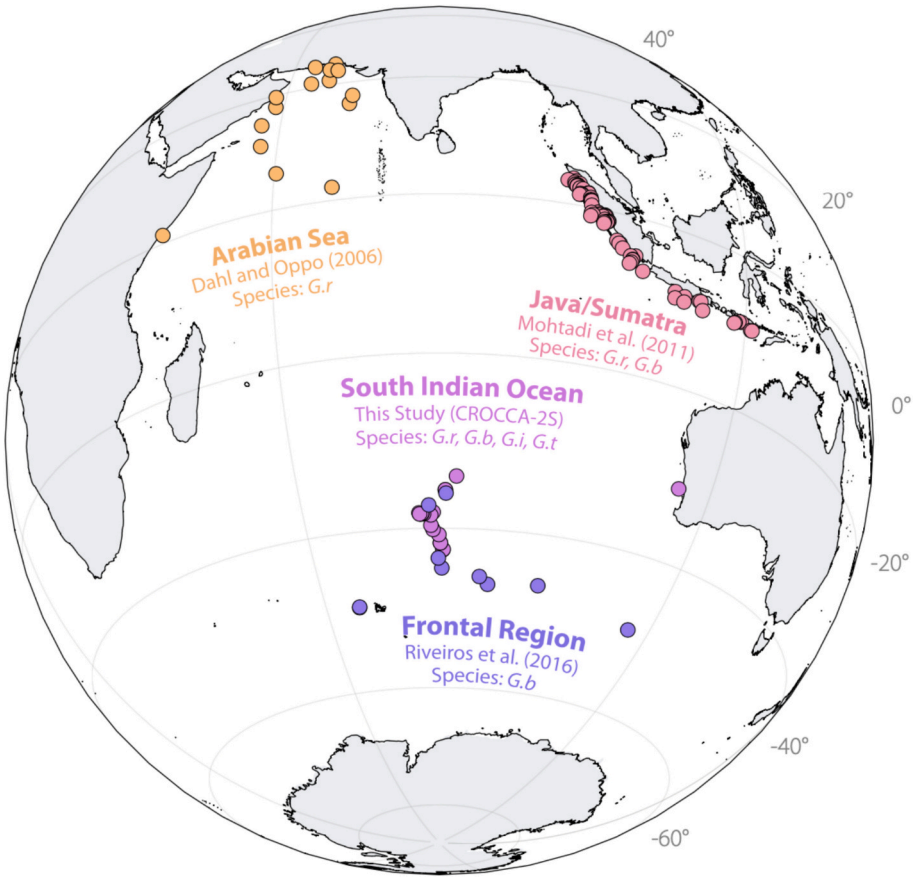

Fig. 1. The locations of the compiled Indian Ocean core tops. Source publications and available species are labeled alongside each major region. Species abbreviations: *Globigerinoides ruber* (*G.r*), *Globigerina bulloides* (*G.b*), *Globorotalia inflata* (*G.i*), and *Globorotalia truncatulinoides* (*G.t*).

prior to analysis. *G. ruber* and *G. bulloides* samples were analyzed on a Finnigan MAT-252 isotope ratio mass spectrometer (IRMS) with a Kiel III device at the University of Florida, while *G. inflata* and *G. truncatulinoides* were run on an Finnigan MAT-253 Plus IRMS with a Kiel IV device at the City University of New York's Advanced Science Research Center. Repeated measurement of the NBS-19 standard returned average values of −2.20 ‰ ($n = 86$) and − 2.19 ‰ ($n = 13$) for Florida and New York, respectively, indicating no significant offset between the two facilities. The long-term analytical reproducibility across the six-month analysis period is 0.06 ‰ and 0.05 ‰ (1σ) for Florida and New York, respectively.

For minor and trace element analyses, approximately 600 μg of foraminiferal tests was equally portioned into two microcentrifuge vials, submerged in ultra-pure water, and gently crushed with a thin plastic rod to open the chambers. Foraminifera were cleaned following an established protocol that included: (1) sonication in water and methanol to remove clay material; (2) treatments in hot reducing and oxidizing solutions to remove remnant authigenic coatings and organic material; (3) transferal to acid-leached vials; and (4) a final weak acid leach in a 0.001 N nitric acid solution (Lea et al., 2000). All clean work was conducted in a laminar flow bench under trace metal clean conditions. Cleaned samples were analyzed for Mg, Al, Mn, Fe, Sr, and Ca using a Thermo Scientific Element XR high-resolution inductively coupled plasma mass spectrometer (HR-ICP-MS) at Old Dominion University. We employed a standard external calibration approach where a series of five calibration standards and two nitric acid blanks were measured every six samples in the run sequence. Long-term analytical precision across all runs was 2.56 %, 0.63 %, and 0.75 % (1σ) for three consistency standards with known Mg/Ca ratios of 1.44, 3.54, and 5.77 mmol/mol, respectively ($n = 5$). Samples that reported Al/Ca, Mn/Ca, or Fe/Ca ratios >150 μmol/mol indicate insufficient cleaning and were rejected.

2.3. Refining calcification depth and identifying calibration parameters

The environmental dataset used to develop our calibrations was assembled by indexing WOA18 and GLODAP data from each species' apparent calcification depth (ACD). We estimated ACD at each core location by aligning the observed core top $\delta^{18}O$ ($\delta^{18}O_c$) for each species against site-specific profiles of predicted equilibrium $\delta^{18}O$ ($\delta^{18}O_{eq}$). This approach is preferred to other potential indicators of depth habitat (e.g., food availability) because it directly relates measurable geochemistry to physical ocean conditions while simultaneously allowing for the propagation of uncertainties related to empirical relationships between shell and seawater chemistry. We calculate $\delta^{18}O_{eq}$ profiles using WOA18 temperature and salinity data averaged across each species' growth season inferred from nearby sediment traps (Curry et al., 1992; King and Howard, 2001; Mohtadi et al., 2009; Northcote and Neil, 2005) and an analysis of global shell flux patterns (Jonkers and Kučera, 2015). A summary of the seasonality imposed on each species is summarized in Table 2.

To compute $\delta^{18}O_{eq}$, we first estimate the $\delta^{18}O$ composition of seawater ($\delta^{18}O_{sw}$) using WOA18 salinity profiles. Salinity and $\delta^{18}O_{sw}$ are linearly related throughout much of the global ocean, although the structure of this relationship can vary by latitude (e.g., LeGrande and Schmidt, 2006) as well as regionally within a latitudinal band (e.g., Glaubke et al., 2024). We therefore selected a set of regionally distinct equations for each major ocean region represented in our dataset (see Supporting Information) to translate salinity into $\delta^{18}O_{sw}$. We then combined the computed $\delta^{18}O_{sw}$ profiles with WOA18 temperature data to estimate $\delta^{18}O_{eq}$ using established $\delta^{18}O$-temperature equations (see

Table 1
Location and geochemical results for new sediments core tops from the CROCCA-2S expedition.

Core	Latitude (°N)	Longitude (°E)	Depth (m)	Mean Age (yrs BP)	*G. ruber* $\delta^{18}O_c$ (‰ VPDB)	*G. ruber* Mg/Ca (mmol/mol)	*G. bulloides* $\delta^{18}O_c$ (‰ VPDB)	*G. bulloides* Mg/Ca (mmol/mol)	*G. inflata* $\delta^{18}O_c$ (‰ VPDB)	*G. inflata* Mg/Ca (mmol/mol)	*G. truncat.* $\delta^{18}O_c$ (‰ VPDB)	*G. truncat.* Mg/Ca (mmol/mol)
TT1811-04MC	−31.29	114.56	2675	5995	−0.63	–	–	–	0.05	1.57	0.58	1.73
TT1811-30GGC	−42.54	80.54	2936	2936	0.54	–	1.37	1.74	1.24	1.49	1.22	1.36
TT1811-31MC	−42.48	80.59	2981	2981	0.59	–	1.22	1.55	1.80	1.64	1.08	1.44
TT1811-32MC	−41.72	80.16	3174	3174	–	–	0.69	1.94	1.10	1.50	1.28	1.40
TT1811-34GGC	−41.72	80.16	3167	3167	–	–	1.36	–	1.12	1.31	0.96	1.38
TT1811-36MC	−40.75	79.93	3035	3035	0.33	1.70	0.77	–	1.25	1.33	1.05	1.28
TT1811-38MC	−40.16	79.06	2845	2845	0.21	–	0.62	1.80	1.02	1.54	0.93	1.55
TT1811-40MC	−39.66	78.76	2954	3314	0.01	1.58	0.84	2.04	1.14	1.44	1.09	1.30
TT1811-43MC	−38.15	79.11	1796	2959	0.87	1.62	1.54	1.80	0.91	1.51	0.59	1.55
TT1811-45MC	−38.48	78.75	2034	190	−0.09	1.67	0.63	1.99	0.88	1.46	0.94	1.48
TT1811-50GGC	−38.34	77.71	1118	436	−0.15	–	0.89	–	1.00	1.64	0.72	1.56
TT1811-53MC	−38.35	77.37	1998	1780	0.26	1.67	0.55	2.01	0.65	1.50	0.72	–
TT1811-56GGC	−38.31	77.48	1635	3780	0.18	–	0.36	–	0.62	1.71	0.63	1.54
TT1811-59MC	−38.34	77.21	2369	617	0.09	1.68	0.48	1.89	0.79	1.44	0.83	1.46
TT1811-60MC	−38.30	77.42	1930	4189	0.22	1.77	0.69	2.09	1.60	1.69	0.69	1.52
TT1811-63GGC	−38.21	77.05	2680	2113	0.02	1.83	0.77	–	0.66	1.49	0.97	1.35
TT1811-65MC	−38.34	77.13	2568	1810	−0.01	–	0.71	2.03	1.05	1.58	1.05	1.38
TT1811-71GGC	−35.59	80.84	2598	6098	0.04	1.72	0.93	1.78	0.82	1.60	0.93	–
TT1811-72MC	−35.59	80.84	2598	3036	0.11	1.59	0.82	2.13	0.95	1.50	1.37	1.41
TT1811-74MC	−34.01	82.35	3512	5310	0.61	1.58	1.26	1.44	1.10	1.26	1.16	1.06

Table 2
An ecological summary of the species under investigation.

Species	Morphotype	Conventional Depth Habitat	Seasonality	References
Globigerinoides ruber	sensu lato	~30–70 m	**N of 30°S:** Year-round **S of 30°S:** Austral Summer (DJF)	Wang (2000); Schmitt et al. (2019); Jonkers and Kučera (2015)
Globigerina bulloides	–	~0–60 m	**Java/Sumatra:** SE Monsoon (JJASON) **Southern Subtropics:** Austral Spring (SON)	Schiebel and Hemleben (2017); King and Howard (2001); Mohtadi et al. (2009)
Globorotalia inflata	–	~0–300 m (Upper thermocline; highly variable)	Austral Spring/Early Summer (SOND)	Rebotim et al. (2019); King and Howard (2001); Northcote and Neil (2005)
Globorotalia truncatulinoides	sinistral coiling	~0–500 m (Lower thermocline; varies by latitude/season)	Austral Fall/Winter (MAMJJA)	Hemleben et al. (1985); Rebotim et al. (2019); Northcote and Neil (2005); Jonkers and Kučera (2015)

Supporting Information). Finally, we aligned our $\delta^{18}O_c$ observations against each core top's respective $\delta^{18}O_{eq}$ profile. The depth at which they overlap is considered that species' ACD range. Temperature, salinity, nutrient concentrations, and carbon system parameters were indexed from these depths and were either retained for use in the calibration (temperature, salinity, pH) or used to compute carbonate ion concentration ($[CO_3^{2-}]$) using the *PyCO2SYS* package in python (Humphreys et al., 2021). We also computed carbonate saturation (ΔCO_3^{2-}) at the depth of each core to serve as a potential dissolution correction term. However, the lack of any observable relationship with Mg/Ca or threshold behavior below ~30 μmol/kg (e.g., Regenberg et al., 2014) suggests minimal influence from dissolution (Fig. S2), and

so we exclude the term from our calibration exer. Analytical error, replicate error (where available), and coefficient error in the $\delta^{18}O_{sw}$--salinity regressions are propagated forward as uncertainties in estimated calcification depths and calibration parameters using the *uncertainties* package in python (Lebigot, 2022).

2.4. Model calibration

We evaluated the influence of temperature, salinity, pH, and $[CO_3^{2-}]$ on the Mg/Ca of each species by fitting and assessing a suite of multivariate regression models. First, we developed conventional temperature-only calibrations by fitting a weighted least squares regression against log-transformed Mg/Ca. We then iteratively added nonthermal parameters in various combinations assuming their influence on Mg/Ca follows an exponential form, as demonstrated in previous studies (e.g., Gray et al., 2018; Gray and Evans, 2019; Hönisch et al., 2013; Khider et al., 2015; Kısakürek et al., 2008). The full expression of the general Mg/Ca model being tested is as follows:

$$Mg/Ca = \exp.\left(a^{*}(T-25) + b^{*}(S-35) + c^{*}(pH-8) + d^{*}\left(\left[CO_3{}^{2-}\right] - 150\right) + e\right) \quad (1)$$

where coefficients *a* through *d* represent the sensitivity of Mg/Ca to its corresponding parameter and *e* represents the constant. Values are centered using averages for the upper ocean (0–500 m) to avoid nonessential multicollinearity (e.g., Dalal and Zickar, 2012). Each coefficient is tested against the null hypothesis that it has no influence over foraminiferal Mg/Ca via a two-tailed *t*-test with a 95 % confidence threshold ($\alpha = 0.05$). Uncertainties on each coefficient are estimated through a bootstrapping approach where the environmental data for each core top observation are allowed to vary within their 1σ errors with each iteration ($n = 5000$).

For all regressions, we computed the coefficient of determination (R^2) and normalized root mean square error (NRMSE) as core metrics for model fit and performance, respectively. To guard against overfitting, we evaluate these model fit statistics within the context of each model's Bayes factor, a method first developed by Holland et al. (2020). A Bayes factor is a likelihood ratio between two competing models that quantifies the strength of the evidence provided by a dataset in favor of one model over another (Johnson et al., 2023; Kass and Raftery, 2012). By default, this calculation weighs the likelihood that a proposed model is true relative to a null hypothesis that no parameters sufficiently explain the data. The result can be any positive number, with values above 1 expressing support for the proposed model and values below 1 expressing support for the null hypothesis (Lee and Wagenmakers, 2014). More importantly, Bayes factors consider a model's fit (R^2) and number of covariates, "rewarding" models with high goodness-of-fit while simultaneously "penalizing" the inclusion of additional parameters (Jefferys and Berger, 1992). As a result, only multivariate models that sufficiently increase model fit to overcome the penalty of an additional parameter will return a Bayes factor higher than the simpler temperature-only model. Since all models are tested against the same null hypothesis, Bayes factors from any two models can be ratioed together to directly compare their relative likelihoods (K) (Holland et al., 2020; Rouder et al., 2013). In our analysis, we identify the "best" model as the model with the highest Bayes Factor. We then assess and report the likelihood of all other models relative to the "best" model using the framework established by Kass and Raftery (2012), which describes the evidence against an alternate model as either "decisive" ($K > 100$), "strong" ($K = 10$–100), "substantial" ($K = 3.2$–10), or "not worth a bare mention" ($K = 1$–3.2).

We note, however, that Bayes factors are, to some extent, blind to the presence of collinearity among model parameters. It is therefore possible for our analysis to promote calibrations that increase model fit but also contain collinearity that undermines confidence in the coefficient estimates. To counter this, each parameter is assigned a variance inflation factor (VIF), which reports how much of its standard error is inflated as the result of another parameter's inclusion in the model. VIF ranges from 1 upwards and is equal to the square of the increase in standard error (Belsley et al., 1980). While there is debate in the literature as to what VIF threshold corresponds to an unacceptable level of collinearity (e.g., O'brien, 2007), a VIF of 4, equivalent to a doubling of the standard error, is typically viewed as a conservative cut-off value (Miles and Shevlin, 2001).

Altogether, the ideal calibration model should explain the most variance in our Mg/Ca data (high R^2) with the fewest statistically significant covariates (high Bayes factor; *p*-values <0.05) and minimal influence from collinearity (VIF ~ 1).

3. Results

Results from the new CROCCA-2S core tops are shown in Table 1, and the full range of core top $\delta^{18}O_c$ and Mg/Ca (alongside indexed environmental parameters from each species' ACD; discussed below) is summarized in Table 3. On average, *G. ruber* and *G. bulloides* report the most negative $\delta^{18}O_c$ values (−2.38 ‰ and − 1.32 ‰, respectively) and highest Mg/Ca ratios (4.76 mmol/mol and 5.11 mmol/mol, respectively). Both species also exhibit the broadest range in $\delta^{18}O_c$ (−3.86–0.87 ‰ and − 3.35–2.69 ‰, respectively) and Mg/Ca (1.58–6.69 mmol/mol and 1.29–9.86 mmol/mol, respectively) owing to their representation by core tops spanning the high-latitude subtropical ocean, low-latitude marginal seas, and a coastal upwelling region. Consequently, the range in temperature (~3–29 °C), salinity (~33.3–36.7 PSU), pH (~7.92–8.13), and $[CO_3^{2-}]$ values (~118–254 μmol/kg) are similarly broad.

G. inflata and *G. truncatulinoides* reported similar shell chemistries and were generally more positive in $\delta^{18}O_c$ (0.99 ‰ and 0.95 ‰, respectively) and lower in Mg/Ca (1.51 mmol/mol and 1.73 mmol/mol, respectively) than the surface-dwelling species. Both exhibit a notably narrower range of $\delta^{18}O_c$ (0.05–1.80 ‰ and 0.58–1.37 ‰, respectively) and Mg/Ca (1.26–1.71 mmol/mol and 0.58–1.37 mmol/mol, respectively) as they are solely represented by core top samples collected from the south Indian Ocean (Fig. 1). Consequently, temperature (~10–18 °C), salinity (~34.7–35.7 PSU), pH (~8.04–8.13), and $[CO_3^{2-}]$ values for these species (~142–186 μmol/kg) are much narrower than those indexed for *G. ruber* and *G. bulloides* (Table 3).

The relationships between Mg/Ca and environmental parameters are evaluated in section 4.2.

4. Discussion

4.1. Apparent calcification depths

4.1.1. Surface-dwellers

The $\delta^{18}O_c$ values for *G. ruber* and *G. bulloides* largely align with predicted $\delta^{18}O_{eq}$ values within the upper 100 m of each location (Fig. 2). This assessment is consistent with decades of ecological research suggesting both species primarily dwell in the upper mixed layer (e.g., Fairbanks et al., 1980, 1982; Kuroyanagi and Kawahata, 2004; Rebotim et al., 2017). *G. ruber* is more widely distributed throughout this depth window, coalescing around a median ACD of 61 m. This ACD is ~10–30 m deeper than the near-surface habitat often inferred for *G. ruber* (e.g., Farmer et al., 2007) but is consistent with studies suggesting the sensu lato morphotype occupies a deeper ecological niche than its sensu stricto counterpart (~30–70 m; Schmitt et al., 2019). The distribution of *G. bulloides* ACDs is more concentrated towards the near-surface environment, with a median ACD of 4 m (Fig. 2). Most observations (83 %) fall within the 0–30 m depth range, which is supported by abundances observed in plankton tow studies (Peeters and Brummer, 2002). This depth distribution reflects the species' opportunistic feeding behavior and their association with algal blooms in the surface of seasonally productive waters like the monsoon-influenced Java/Sumatran coast

Table 3
The range in $\delta^{18}O_c$, Mg/Ca, and indexed environmental parameters for each species.

Species	$\delta^{18}O_c$ (‰ VPDB)	Mg/Ca (mmol/mol)	T (°C)	S (PSU)	pH	$[CO_3^{2-}]$ (μmol/kg)
G. ruber	−3.86–0.87	1.58–6.69	10.6–29.2	33.7–36.6	7.92–8.13	136–254
G. bulloides	−3.35–2.69	1.29–9.86	3.52–29.3	33.3–35.3	8.02–8.13	118–249
G. inflata	0.05–1.80	1.26–1.71	9.98–16.8	34.8–35.7	8.04–8.13	142–186
G. truncatulinoides	0.58–1.37	1.06–1.73	11.9–14.7	34.7–35.4	8.06–8.13	154–183

and the high-latitude ocean (e.g., Mortyn and Charles, 2003; Sautter and Thunell, 1991; Schiebel et al., 2017).

Notably, there are several core top observations from the south Indian Ocean (this study; Riveiros et al., 2016) that return anomalously deep ACDs (>200 m) for both surface-dwelling species. While these estimates are not outside the range of possibility for *G. bulloides*—specimens have been observed below ~300 m in subantarctic waters (Mortyn and Charles, 2003)—it is more likely that these ACDs are in part a result of deep mixing in the southeast Indian Ocean. The combination of wind-induced Ekman pumping and increased mesoscale eddy activity promotes a generally homogenous upper water column in the region (Koch-Larrouy et al., 2010; Sallée et al., 2006), resulting in $\delta^{18}O_{eq}$ profiles with little vertical structure in the upper ocean (Fig. 2). In the case of *G. bulloides*, these estimated profiles are nearly vertical down to ~600 m. Consequently, small differences in $\delta^{18}O_c$ could lead to large changes in estimated ACD. Analytical error on the $\delta^{18}O_c$ observations (error bars in Fig. 2) places relatively large uncertainties on these deep ACDs (±50–200 m). Fortunately, the consistency in hydrographic conditions with depth ensures these large ACD uncertainties are associated with relatively small ranges in the environmental parameters used in our calibration.

4.1.2. Subsurface-dwellers

The comparatively more positive $\delta^{18}O_c$ values and lower Mg/Ca ratios for *G. inflata* and *G. truncatulinoides* have been taken as a reflection of the species' deeper dwelling habitat in colder waters below the thermocline (e.g., Groeneveld et al., 2019; LeGrande et al., 2004). However, when aligned against our estimated $\delta^{18}O_{eq}$ profiles, estimated ACDs are notably shallow, although none that are anomalous for both *Globorotaliid* species. Most ACDs for *G. inflata* (80 %) fall within the upper 50 m of the water column, with a few observations extending below 100 m to as deep as 500 m. These results do not change if we employ the Epstein and Mayeda (1953) $\delta^{18}O$ – temperature relationship in lieu of the Shackleton (1974) equation, as suggested by King and Howard (2005) (not shown). These ACDs agree with plankton tow results suggesting *G. inflata* abundances are most heavily concentrated in the lower mixed layer/upper thermocline (e.g., Cléroux et al., 2007; Fairbanks et al., 1980; Rebotim et al., 2017). *Globorotalia truncatulinoides* ACDs are mostly concentrated within the upper 150 m of the water column, with two core tops returning ACDs closer to ~300 m. A median ACD of 55 m is comparable to what has been observed in plankton tows and sediment trap studies (e.g., Ravelo and Fairbanks, 1992; Rebotim et al., 2017; Reynolds et al., 2018; Salmon et al., 2016) but is shallower than the lower-thermocline habitat inferred from lower-latitude core top studies (e.g., Anand et al., 2003; Cléroux et al., 2009; Mulitza et al., 1997; Regenberg et al., 2009).

These findings confirm earlier speculations that as the thermocline shoals poleward, *Globorotaliid* species should occupy a shallower depth range than what is inferred from the deeply stratified subtropical ocean (Hemleben et al., 1985). Studies have shown this habitat shoaling to be true in the well-mixed winter water column of the North Atlantic (Cléroux et al., 2008; Durazzi, 1981). Additionally, work has demonstrated that *G. truncatulinoides* $\delta^{18}O_c$ is increasingly correlated to surface ocean temperatures moving south across the subtropical convergence of the south Indian Ocean (Williams and Healy-Williams, 1980). Both species may therefore be less strictly recorders of thermocline conditions in the south Indian Ocean and instead capture mixed layer signals like those recorded by surface-dwellers (e.g., Glaubke et al., 2025).

4.2. Mg/Ca calibration models

4.2.1. G. ruber

For *G. ruber*, two of seven candidate models returned coefficients that were all statistically significant (Fig. 3a). The "best" model with the highest Bayes Factor was the temperature-only equation (colored square in Fig. 3a; Table 4):

$$Mg/Ca = \exp.(0.086 \pm 0.002^{*}(T–25) + 1.49 \pm 0.01) \quad (2)$$

This model indicates an apparent temperature sensitivity of 8.6 ± 0.2 % per °C that falls squarely within the 8–10 % range reported in the literature (e.g., Anand et al., 2003; Dekens et al., 2002; Hollstein et al., 2017; Khider et al., 2015; Kısakürek et al., 2008; Lea et al., 1999). Without the addition of other variables, the temperature-only equation explains 94 % of the observed variance in the core top Mg/Ca data, with a NRMSE of 7.1 %. The other statistically significant model is a multivariate regression that includes a sensitivity to pH of −5.7 ± 2.3 % per 0.1 pH units (outlined square in Fig. 3a):

$$Mg/Ca = \exp.(0.083 \pm 0.002^{*}(T–25) – 0.569 \pm 0.230^{*}(pH–8) + 1.51 \pm 0.02) \quad (3)$$

The large uncertainty associated with this coefficient may be a result of the narrow range of values covered by the *G. ruber* calibration dataset (~0.21; Table 3). All other models incorporating a salinity or $[CO_3^{2-}]$ influence, or some combination thereof, returned statistically insignificant coefficient estimates (Fig. 3a). Likelihood ratios for these models suggests they are "significantly" to "decisively" less probable than the temperature-only model (Table 4).

The apparent pH sensitivity reported in the *G. ruber* multivariate regression is lower than, although within error of, estimates determined from culture experiments (Evans et al., 2016; Gray and Evans, 2019; Kısakürek et al., 2008) and other field calibrations (Gray et al., 2018). Most of these works find that the addition of a pH term significantly reduces the apparent temperature sensitivity of *G. ruber* Mg/Ca from 8 to 10 % per °C to ~6–7 % per °C. While the exact mechanism by which pH directly influences foraminiferal Mg/Ca is still unknown (see, e.g., Allen et al., 2016), this differential implies that the conventional sensitivities from prior studies include some unaccounted-for influence from pH, likely through temperature's influence on the dissociation constant of water (Gray et al., 2018; Gray and Evans, 2019). In our models, the inclusion of the pH term in our analysis does not substantially change apparent temperature sensitivity (8.3 ± 0.2 % per °C) relative to the temperature-only model (8.6 ± 0.2 % per °C) and only marginally improves model fit (R^2 = 94.6 %) and performance (NRMSE = 6.7 %). Moreover, the temperature bias induced by pH changes (−0.65 °C per 0.1 change in pH) is fully encompassed within the uncertainty on the temperature-only calibration. In the modern global ocean, where local variations in pH can approach ~ ± 0.2 (Pelejero et al., 2005), a potential bias of ~1.2 °C is roughly equivalent to the model's standard error of estimate (±1.26 °C; 95 % CI). Even if we consider pH changes over the last major example of global climate change—the Last Deglaciation—where colder ocean temperatures and lower atmospheric CO_2 increased pH by ~0.15 (Gray and Evans, 2019), the resulting bias to reconstructed

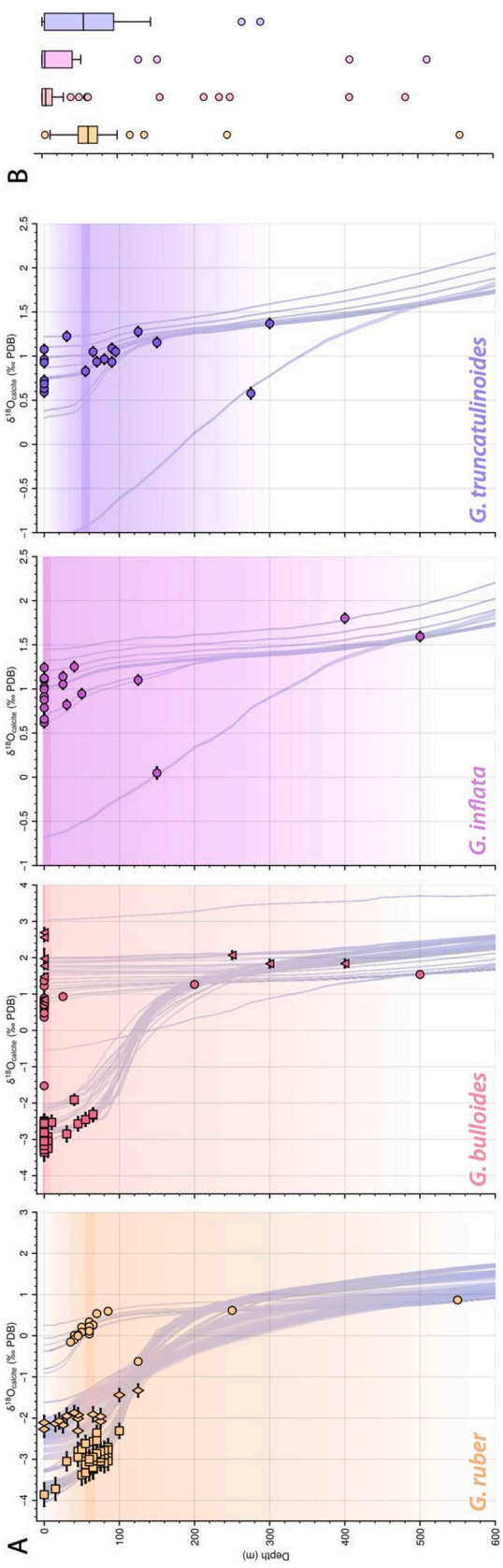

Fig. 2. $\delta^{18}O_c$-derived estimates of site-specific apparent calcification depth (ACD) for each planktic foraminiferal species (colored markers). Horizontal black error bars represent the analytical uncertainty on the $\delta^{18}O_c$ measurement. Gray lines represented predicted equilibrium $\delta^{18}O$ computed using seasonal temperature and salinity observations from each core site (see seasonal bias imposed for each species in Table 1). The thickness of the gray line represents the uncertainty associated with the calculations. The median and range each species' ACD is marked by the bold colored horizontal bars and fading background colour, respectively. ACD estimates from (A) are represented as a box-and-whisker plots in (B).

(caption on next column)

temperatures (~1 °C) would still be within calibration error. Consequently, there is insufficient evidence to conclude that the use of a multivariate calibration substantially improves on the use of the simpler temperature-only calibration, at least for this regional *G. ruber* dataset. However, in light of culture experiments that find carbonate influences on *G. ruber* Mg/Ca under constant temperatures (e.g., Allen et al., 2016; Evans et al., 2016; Kısakürek et al., 2008), we suggest future Indian Ocean calibrations include sites where temperature and pH (and $[CO_3^{2-}]$) can be decoupled to better assess their independent influences on Mg/Ca.

4.2.2. *G. bulloides*

For *G. bulloides*, three calibration models returned coefficients that were all statistically significant (Fig. 4). Two of the three models were similar to the results above: a temperature-only equation and a multivariate regression including the influence of pH (bordered squares in Fig. 4a):

$$Mg/Ca = \exp.(0.077 \pm 0.002^{*}(T–25) + 1.68 \pm 0.02) \quad (4)$$

$$Mg/Ca = \exp.(0.075 \pm 0.002^{*}(T–25) – 1.61 \pm 0.619^{*}(pH–8) + 1.82 \pm 0.06) \quad (5)$$

The equations return an apparent temperature sensitivity of 7.7 ± 0.2 % and 7.5 ± 0.2 % per °C that is within the 6–8 % range typically reported for this species (e.g., Cléroux et al., 2008; Gray et al., 2018; Marr et al., 2011). As with *G, ruber*, the addition of the pH term does not significantly modify apparent temperature sensitivity and only marginally improves model fit (R^2 from 96.6 % to 96.9 %) and performance (NRMSE from 5.7 % to 5.6 %) (Fig. 4). Consequently, the multivariate model ranks as a less likely representation of *G. bulloides* Mg/Ca than the temperature-only model (Table 5).

Nevertheless, ranking above these calibrations is the "best" model: a multivariate regression accounting for changes in both temperature and salinity (colored square in Fig. 4a):

$$Mg/Ca = \exp.(0.068 \pm 0.002^{*}(T–25) – 0.187 \pm 0.03^{*}(S–35) + 1.51 \pm 0.03) \quad (6)$$

The model suggests an apparent temperature sensitivity of 6.8 ± 0.2 % per °C, consistent with previous studies (Gray et al., 2018; Gray and Evans, 2019; Saenger and Evans, 2019) but also indicates a considerable sensitive to salinity of −18.7 ± 3.0 % per PSU. This result is surprising for two reasons. First, the magnitude of this estimated sensitivity far exceeds those determined in culture (~4–6 % per PSU; Hönisch et al., 2013; Kısakürek et al., 2008; Lea et al., 1999). High apparent sensitivities have been reported in core top calibrations before (~15–59 % per PSU; Arbuszewski et al., 2010; Ferguson et al., 2008), but these results have since been explained away as a function of variable preservation state (Hertzberg and Schmidt, 2013) or the result of high Mg-calcite overgrowths in hyper saline environments (Hoogakker et al., 2009), neither of which apply to our sample set. Second, our data suggest Mg/Ca is *negatively* correlated to salinity (Fig. 4b), the opposite of what is reported in other works (e.g., Arbuszewski et al., 2010; Dueñas-Bohórquez et al., 2009; Ferguson et al., 2008; Hönisch et al., 2013; Kısakürek et al., 2008; Lea et al., 1999).

A

G. ruber

Model: T, S
Coefficients:
a: 0.086 ± 0.002 (<0.01)
b: 0.009 ± 0.014 (0.56)
e: 1.485 ± 0.011
Model Metrics
R^2 = 0.942 NRMSE = 0.064

Model: T
Coefficients:
a: 0.086 ± 0.002 (<0.01)
e: 1.485 ± 0.011
Model Metrics
R^2 = 0.943 NRMSE = 0.071

Model: T, pH
Coefficients:
a: 0.083 ± 0.002 (<0.01)
c: -0.569 ± 0.230 (0.03)
e: 1.513 ± 0.016
Model Metrics
R^2 = 0.946 NRMSE = 0.067

Model: T, S, pH
Coefficients:
a: 0.082 ± 0.003 (<0.01)
b: -0.019 ± 0.017 (0.32)
c: -0.756 ± 0.287 (0.03)
e: 1.520 ± 0.017
Model Metrics
R^2 = 0.947 NRMSE = 0.067

Model: T, [CO_3^{2-}]
Coefficients:
a: 0.089 ± 0.003 (<0.01)
d: -0.001 ± 0.001 (0.23)
e: 1.539 ± 0.042
Model Metrics
R^2 = 0.943 NRMSE = 0.066

Model: T, S, [CO_3^{2-}]
Coefficients:
a: 0.089 ± 0.003 (<0.01)
b: 0.006 ± 0.014 (0.64)
d: -0.001 ± 0.001 (0.25)
e: 1.539 ± 0.042
Model Metrics
R^2 = 0.943 NRMSE = 0.065

Model: T, S, pH, [CO_3^{2-}]
Coefficients:
a: 0.077 ± 0.006 (<0.01)
b: -0.027 ± 0.020 (0.35)
c: -1.056 ± 0.435 (0.05)
d: 0.001 ± 0.001 (0.33)
e: 1.479 ± 0.048
Model Metrics
R^2 = 0.947 NRMSE = 0.061

B

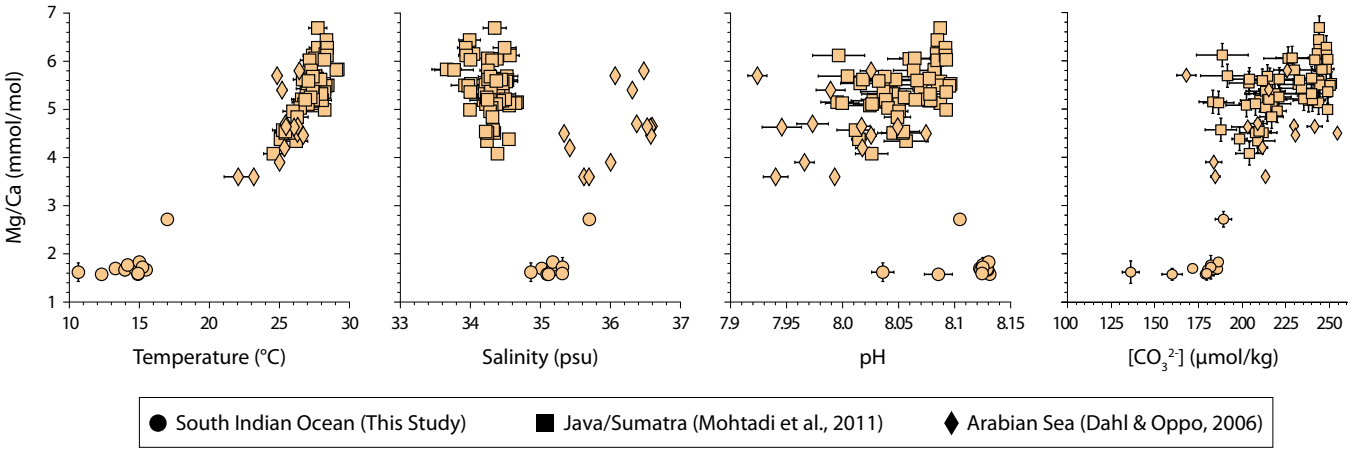

Fig. 3. Multivariate regression results and Mg/Ca-parameter relationships for *G. ruber*. (A) Coefficient estimates and model fit statistics for each investigated multivariate regression (solid squares) and the temperature-only regression (hashed square). Included model parameters are listed at the top of each square. Coefficients correspond to the variables in Eq. (1). Estimates represent the average and 1σ standard deviation of 5000 Monte Carlo realizations. Values in parentheses represent the *p*-values for each coefficient. The "best" model, identified by the highest Bayes factor (Table 4), is colored yellow. Other models that return fully significant coefficients but rank below the "best" model are indicated by the yellow borders. (B) Individual relationships between Mg/Ca and temperature, salinity, pH, and [CO_3^{2-}]. Vertical error bars represent the analytical and replicate error (where available) for each Mg/Ca observation. Horizontal error bars represent uncertainty in each parameter related to uncertainty in each species' ACD. Markers represent different regions (see legend). (For interpretation of the references to colour in this figure legend, the reader is referred to the web version of this article.)

Table 4
Bayes Factors and Variance Inflation Factors for *G. ruber* Calibration Models.

Model	Bayes Factor	K	Evidence Against[a]	Temperature VIF	Salinity VIF	pH VIF	$[CO_3^{2-}]$ VIF
T	$5.33 * 10^{46}$			–	–	–	–
T, S	$1.95 * 10^{45}$	27.3	Not worth a bare mention	1.19	1.19	–	–
T, pH	$2.89 * 10^{46}$	1.85	Strong	1.13	–	1.13	–
T, $[CO_3^{2-}]$	$4.21 * 10^{45}$	12.7	Strong	2.30	–	–	2.30
T, S, pH	$1.86 * 10^{45}$	28.7	Strong	1.80	1.84	1.75	–
T, S, $[CO_3^{2-}]$	$1.70 * 10^{44}$	314	Decisive	2.38	1.22	–	2.35
T, S, pH, $[CO_3^{2-}]$	$1.34 * 10^{44}$	399	Decisive	**16.1**	3.22	**7.91**	**10.6**

Bold VIFs indicate severe collinearity (VIF > 4).
[a] Qualitative interpretation of K relative to "best" model according to framework by Kass and Raftery (2012).

These discrepancies lead us to believe that the salinity sensitivity in our "best" calibration model is an artefact of data clustering rather than a true reflection of the nonthermal controls on *G. bulloides*' Mg/Ca. A closer look at the data reveal two regionally distinct relationships between *G. bulloides* Mg/Ca and salinity (Fig. 4b). At low Mg/Ca ratios, core tops from the south Indian Ocean (this study; Riveiros et al., 2016) show a modest positive trend, whereas higher Mg/Ca ratios from the Java/Sumatran coast (Mohtadi et al., 2011) exhibit a strong negative trend. These correlations reflect fundamentally different hydroclimatic regimes at each location. In the south Indian Ocean, Mg/Ca is related to salinity through its near-perfect covariation with temperature (r = 0.99), which is common in subtropical oceans where temperatures are correlated to the evaporation-precipitation balance at the surface (LeGrande and Schmidt, 2006). In contrast, the negative trend in the Java/Sumatran cores indicates an influence from the southeast Asian monsoon. During the boreal summer and fall, warmer temperatures are associated with increased monsoonal precipitation, yielding an inverse correlation between temperature and salinity ($r = -0.81$). This correlation is reflected in the *G. bulloides* dataset because the species' growth season is heavily biased towards the upwelling conditions promoted by the monsoon's southeasterly winds (Mohtadi et al., 2009). Combining these two regional subsets both creates an artificially large negative correlation between Mg/Ca and salinity ($r = -0.71$) and masks the collinearity between temperature and salinity that would normally flag the salinity coefficient as untrustworthy (VIF ~ 2; Table 5).

Does salinity remain a potent influence over *G. bulloides* Mg/Ca if we conduct separate regression analyses on the two regional subsets? The results suggest that the "best" models for both regions are the temperature-only equations (Figs. S3 and S4). All other models fail to return statistically significant coefficients, although this appears to be due in part to a significant degree of collinearity among the calibration parameters (Tables S3 and S4), particularly in the south Indian Ocean (VIF > 4). For example, the near-perfect correlation between temperature and salinity in the south Indian Ocean (r = 0.99) makes it impossible for our analysis to estimate the relative contribution of either parameter to Mg/Ca. This collinearity therefore limits our ability to conclude with confidence that secondary influences do not have a substantial impact on *G. bulloides* Mg/Ca. Nevertheless, the presence of these regionalities implies that the substantial nonthermal sensitives determined from the full dataset is not a robust parameterization of *G. bulloides* Mg/Ca.

4.2.3. Comparison with published surface-dweller models

Compared to previously published equations (Fig. 5), the calibration models developed for *G. ruber* and *G. bulloides* offer the best empirical fit to our core top compilation (Table 6). For *G. ruber*, most equations tend to overestimate ACD temperature by ~2–4 °C, resulting in generally lower R^2 values, higher NRMSE, and lower Bayes factors (Table 6). The Lea et al. (2000) formulation stands out by its poor fit to our Indian Ocean dataset, as it consistently overestimates ocean temperatures by >5 °C across the full range calibrated here. Meanwhile, the multivariate regression from Gray et al. (2018) underestimates temperatures by ~2–3 °C below ~18 °C, assuming a standard salinity range (33–36 PSU) and average pH for the region (8.1). For *G. bulloides*, all models except for the Anand et al. (2003) "All Planktic" regression are remarkably consistent in their temperature predictions below ~15 °C (Fig. 5b), suggesting each would provide robust reconstructions in the mid-to-high latitude ocean, within error. These equations diverge at higher temperatures, however, with only our temperature-only model reliably fitting the data from the Java/Sumatran coast.

4.2.4. G. inflata and G. truncatulinoides

For the subsurface-dwelling species, the dynamic range of our calibration parameters was too limited to yield robust calibration models. The relatively consistent *G. inflata* Mg/Ca ratios across our narrow calibration range returned no statistically significant coefficients, low R^2 values, and Bayes factors below 1 (Fig. S5 and Table S5). This stands in stark contrast to the environmental relationships documented for this species over a broader range of ocean conditions (e.g., Anand et al., 2003; Cléroux et al., 2008; Elderfield and Ganssen, 2000; Groeneveld and Chiessi, 2011). Results from *G. truncatulinoides* returned two models with ostensibly significant coefficients, but the combination of a limited dynamic range (Table 3) and substantial collinearity between parameters (VIF > 4) yields unrealistic coefficient estimates and large uncertainties (Fig. S5 and Table S6). For these reasons, developing regional calibrations for these species, and assessing their sensitivity to nonthermal parameters, is not possible with the present dataset.

In lieu of developing our own models, we attempted to fit previously published temperature-only equations to our dataset to determine which offers the best predictions of ACD temperature (Figs. 6 and 7). The analysis reveals clear differences in the accuracy of predicted temperatures among the tested models. For example, the Cléroux et al. (2008) equation for *G. inflata* is the only regression to run through the Mg/Ca data (Fig. 8a), yielding temperatures estimates that cluster in proximity to a 1:1 line with ACD temperature (Fig. 6). By comparison, the models from Anand et al. (2003) ("All Planktic" and species-specific) overestimate temperatures by ~2–4 °C, and the equations from Elderfield and Ganssen (2000) and Groeneveld et al. (2019) underestimate temperatures by a similar degree (Fig. 6). *G. truncatulinoides* temperatures are best captured by the equation from McKenna and Prell (2004) developed in the subtropical Indian Ocean (Fig. 7), an indication that regional calibrations may be the most appropriate selection for down-core reconstructions. Equations from Elderfield and Ganssen (2000) and Regenberg et al. (2009), meanwhile, do not fit the core top data (Fig. 8b) and offer the least accurate temperature estimates (Fig. 7).

Despite these differences in the *accuracy* of published equations, the narrow range in temperatures make it difficult to assess their *precision* (Table 6). In all cases, the models tested return R^2 values below 0 and NRMSE values approaching ~30–50 %, in some cases exceeding 100 %. These poor fit statistics likely stem from the fact that the core top data insufficiently captures the curvature of the exponential Mg/Ca-temperature relationship within a limited temperature window. In other words, the "noise" of natural variability in core top Mg/Ca overwhelms the "signal" of the true exponential relationship. While this does not preclude the use of these equations for down-core applications in the south Indian Ocean, it does prohibit an unqualified recommendation of

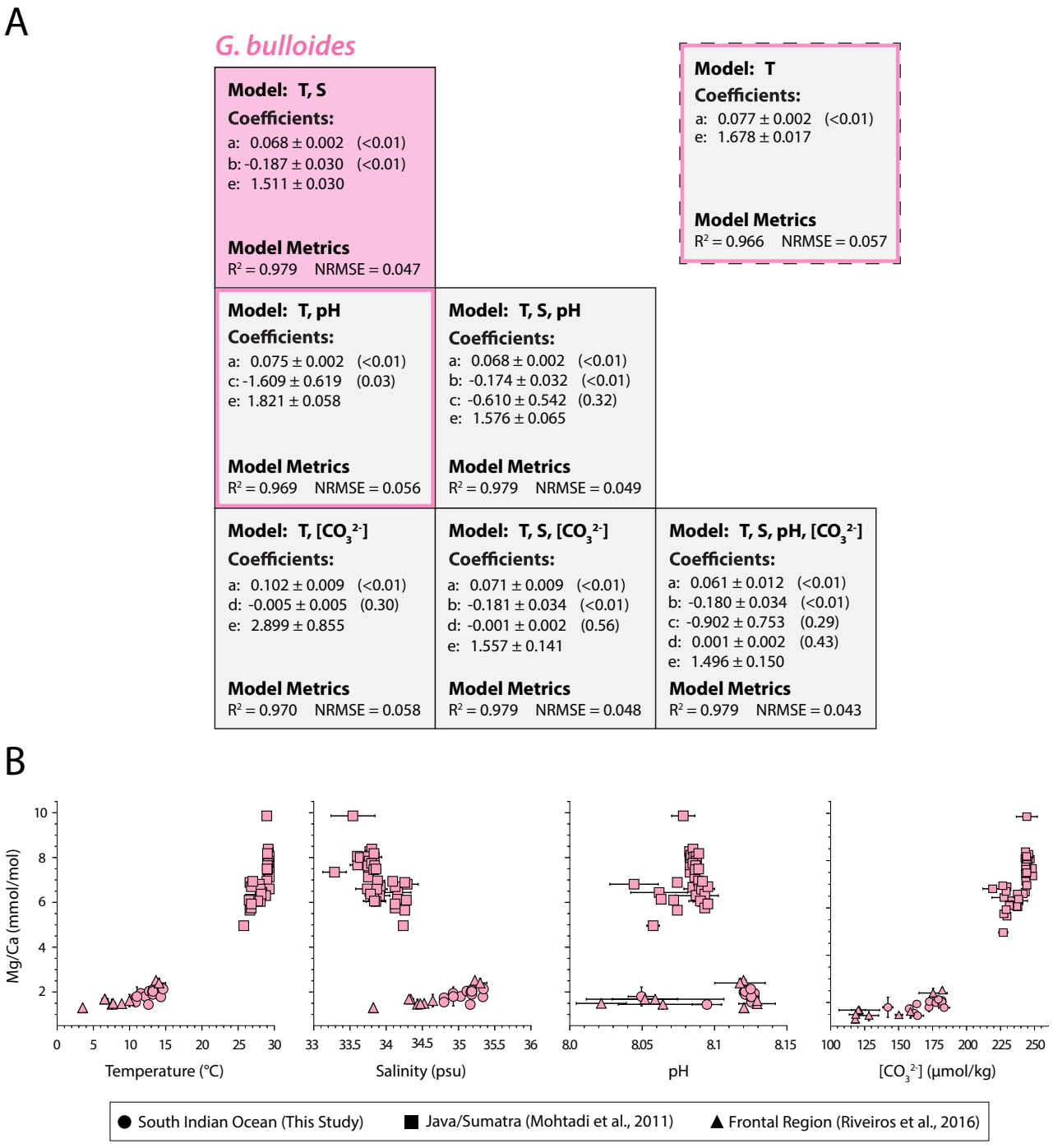

Fig. 4. Multivariate regression results and Mg/Ca-parameter relationships for *G. bulloides*. (A) Coefficient estimates and model fit statistics for each investigated multivariate regression (solid squares) and the temperature-only regression (hashed square). Included model parameters are listed at the top of each square. Coefficients correspond to the variables in Eq. (1). Estimates represent the average and 1σ standard deviation of 5000 Monte Carlo realizations. Values in parentheses represent the *p*-values for each coefficient. The "best" model, identified by the highest Bayes factor (Table 5), is colored pink. Other models that return fully significant coefficients but rank below the "best" model are indicated by the pink borders. (B) Individual relationships between Mg/Ca and temperature, salinity, pH, and $[CO_3^{2-}]$. Vertical error bars represent the analytical and replicate error (where available) for each Mg/Ca observation. Horizontal error bars represent uncertainty in each parameter related to uncertainty in each species ACD. Markers represent different regions (see legend). (For interpretation of the references to colour in this figure legend, the reader is referred to the web version of this article.)

which equation is most appropriate for these species in this region. We therefore recommend the use of classical tests, such as the replication of modern temperatures in core top sediments, to determine which equation should be used for regional reconstructions. We also call for more data from the region to not only provide a robust regional calibration, but also to develop the first multivariate calibrations for these species globally.

5. Conclusions

In this work, we compiled paired Mg/Ca-$\delta^{18}O$ observations from four planktic foraminiferal species across 115 Indian Ocean core tops, which we used to develop temperature-only and multivariate calibration models of Mg/Ca. We used a Bayesian approach to assess whether the inclusion of secondary, nonthermal parameters sufficiently improves the

Table 5
Bayes Factors and Variance Inflation Factors for *G. bulloides* Calibration Models.

Model	Bayes Factor	K	Evidence Against[a]	Temperature VIF	Salinity VIF	pH VIF	$[CO_3^{2-}]$ VIF
T	$8.00 * 10^{41}$	$4.34 * 10^{4}$	Decisive	–	–	–	–
T, S	$3.47 * 10^{46}$			2.03	2.03	–	–
T, pH	$5.17 * 10^{41}$	$6.72 * 10^{4}$	Decisive	1.17	–	1.17	–
T, $[CO_3^{2-}]$	$7.81 * 10^{40}$	$4.45 * 10^{5}$	Decisive	**32.0**	–	–	**32.0**
T, S, pH	$1.80 * 10^{45}$	19.0	Strong	2.04	2.25	1.29	–
T, S, $[CO_3^{2-}]$	$1.10 * 10^{45}$	32.0	Strong	**47.4**	2.54	–	**40.1**
T, S, pH, $[CO_3^{2-}]$	$9.11 * 10^{43}$	381	Decisive	**144**	2.59	3.93	**122**

Bold VIFs indicate severe collinearity (VIF > 4).
[a] Qualitative interpretation of K relative to "best" model according to framework by Kass and Raftery (2012).

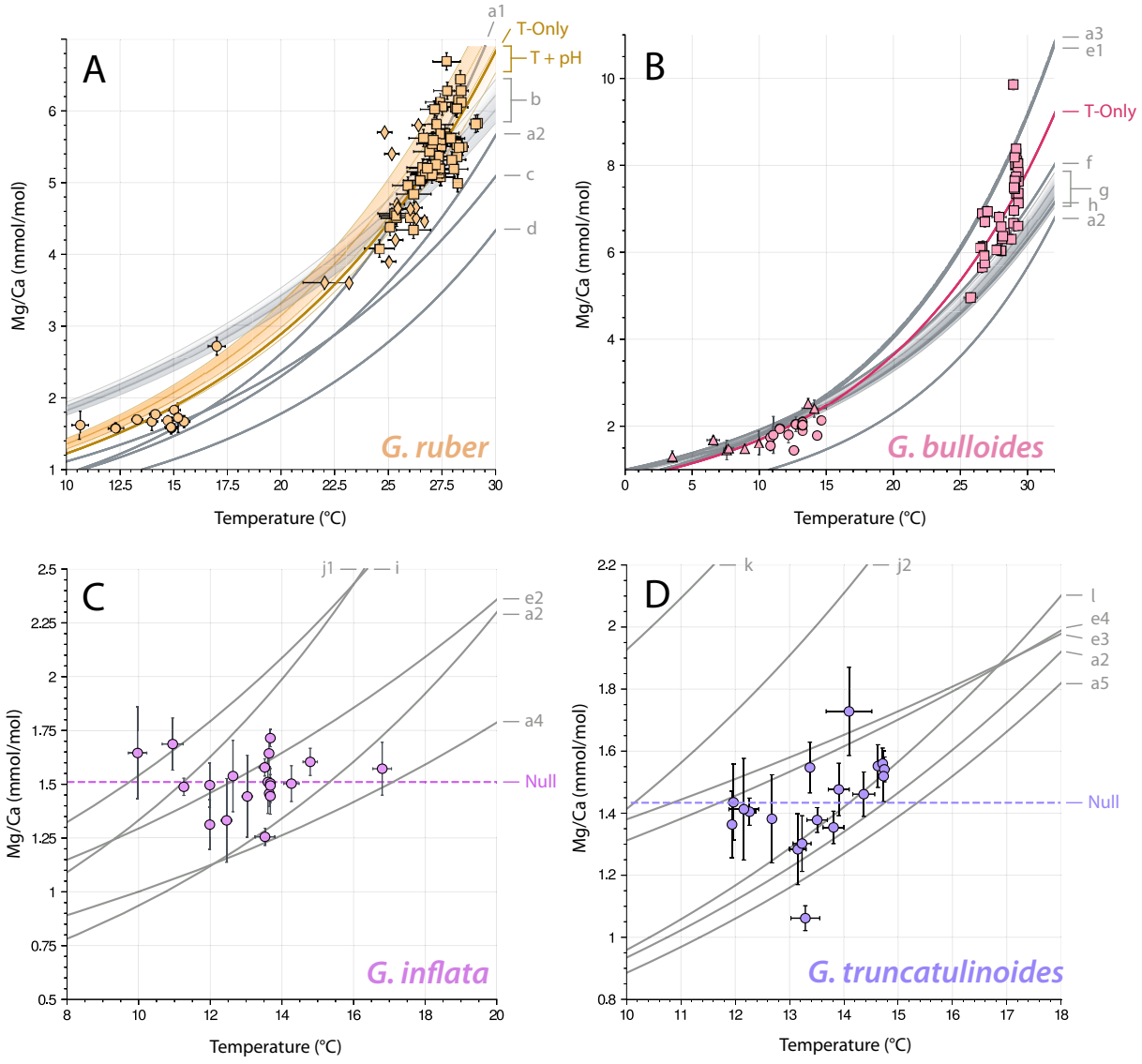

Fig. 5. Comparing developed calibration models (colored regression lines) against previously published models (gray regression lines) for (A) *G. ruber* and (B) *G. bulloides*. Published regressions are denoted with letters that identify their source publication and fit statistics in Table 6. Shaded envelopes represent multivariate regressions under varying secondary influences, where darker shading represents higher values (see Table 6).

fit and performance of calibration models over the classic temperature-only model. For surface-dwelling *G. ruber* (sensu lato), our analysis returned a temperature-only equation with an apparent temperature sensitivity (8.6 ± 0.2 % per °C) that aligns with previously published calibration studies. This equation ranked as the "best" among other multivariate models, including an equation with a minor sensitivity to pH (−5.7 ± 2.3 % per 0.1 pH units). The addition of the pH term did not significantly change our estimate of apparent temperature sensitivity, and the bias introduced by not accounting for pH change is accounted for within the overall calibration uncertainty for the temperature-only model (~ ±1.2 °C; 95 % CI). We suggest that the temperature-only equation offers a sufficiently robust parameterization for *G. ruber* Mg/Ca and should be used for surface temperature reconstructions in the region.

Table 6
Comparing Model Fit Statistics with Previously Published Equations.

Model Label	Original Reference	Notes[a]	Equation	R^2	NRMSE[b]	K[c]
G. ruber						
T-Only ("Best")	This Study	Ssp	Mg/Ca = exp.(0.086*(T – 25) + 1.49)	0.94	0.07	
T + pH	This Study	Multivariate	Mg/Ca = exp.(0.084*(T – 25) – 0.544*(pH – 8) + 1.51)	0.94	0.07	1.85
a1	Anand et al. (2003)	Ssp	Mg/Ca = 0.34*exp.(0.102*T)	0.93	0.07	8.8×10^{3}
a2	Anand et al. (2003)	All Planktic	Mg/Ca = 0.38*exp.(0.090*T)	0.71	0.14	4.2×10^{27}
b	Gray et al. (2018)	Multivariate	Mg/Ca = exp.(0.064*T + 0.033*S – 0.83*(pH – 8) – 0.03)	0.63	0.15	2.0×10^{31}
c	Sadekov et al. (2008)	Ssp	Mg/Ca = 0.52*exp.(0.076*T)	0.45	0.19	2.0×10^{38}
d	Lea et al. (2000)	Ssp	Mg/Ca = 0.30*exp.(0.089*T)	<0	0.29	2.5×10^{51}
G. bulloides						
T-Only	This Study	Ssp	Mg/Ca = exp.(0.068*(T – 25) + 1.51)	0.97	0.06	
a2	Anand et al. (2003)	All Planktic	Mg/Ca = 0.38*exp.(0.090*T)	0.64	0.20	3.1×10^{29}
a3	Anand et al. (2003)	Ssp	Mg/Ca = 0.81*exp.(0.081*T)	0.94	0.08	8.0×10^{5}
e1	Cléroux et al. (2008)	Ssp	Mg/Ca = 0.78*exp.(0.082*T)	0.95	0.08	1.9×10^{4}
f	Riveiros et al. (2016)	Ssp	Mg/Ca = exp.(0.065*T)	0.92	0.09	2.8×10^{9}
g	Gray and Evans (2019)	Multivariate	Mg/Ca = exp.(0.064*T + 0.036*(S – 35) – 0.88*(pH – 8) + 0.15)	0.90	0.11	9.1×10^{12}
h	Marr et al. (2011)	Ssp	Mg/Ca = 0.95*exp.(0.063*T)	0.86	0.12	7.2×10^{16}
G. inflata						BF[d]
a2	Anand et al. (2003)	All Planktic	Mg/Ca = 0.38*exp.(0.090*T)	<0	0.40	1.4×10^{-4}
a4	Anand et al. (2003)	Ssp	Mg/Ca = 0.56*exp.(0.058*T)	<0	0.64	7.7×10^{-7}
e2	Cléroux et al. (2008)	Ssp	Mg/Ca = 0.71*exp.(0.060*T)	<0	0.30	2.2×10^{-3}
i	Groeneveld and Chiessi, 2011	Ssp	Mg/Ca = 0.72*exp.(0.076*T)	<0	0.57	1.3×10^{-6}
j1	Elderfield and Ganssen (2000)	Ssp	Mg/Ca = 0.49*exp.(0.10*T)	<0	0.37	3.0×10^{-4}
G. truncatulinoides						
a2	Anand et al. (2003)	All Planktic	Mg/Ca = 0.38*exp.(0.090*T)	<0	0.58	6.0×10^{-4}
a5	Anand et al. (2003)	Ssp	Mg/Ca = 0.36*exp.(0.090*T)	<0	0.73	5.1×10^{-5}
e3	Cléroux et al. (2008)	Ssp	Mg/Ca = 0.88*exp.(0.045*T)	<0	1.20	2.8×10^{-7}
e4	Cléroux et al. (2008)	Mixed Deep	Mg/Ca = 0.78*exp.(0.052*T)	<0	0.90	8.5×10^{-6}
j2	Elderfield and Ganssen (2000)	Ssp	Mg/Ca = 0.52*exp.(0.10*T)	<0	1.23	1.8×10^{-7}
k	Regenberg et al. (2009)	Mixed Deep	Mg/Ca = 0.84*exp.(0.083*T)	<0	2.50	1.1×10^{-11}
l	McKenna and Prell (2004)	Ssp	Mg/Ca = 0.36*exp.(0.098*T)	<0	0.42	1.3×10^{-2}

[a] Ssp = "Species-specific".
[b] NRMSE represents the root mean square error normalized to the dataset's range.
[c] K values are relative to models determined in this study (listed first).
[d] BF values are relative to the null hypothesis (horizontal line through the mean of the data).

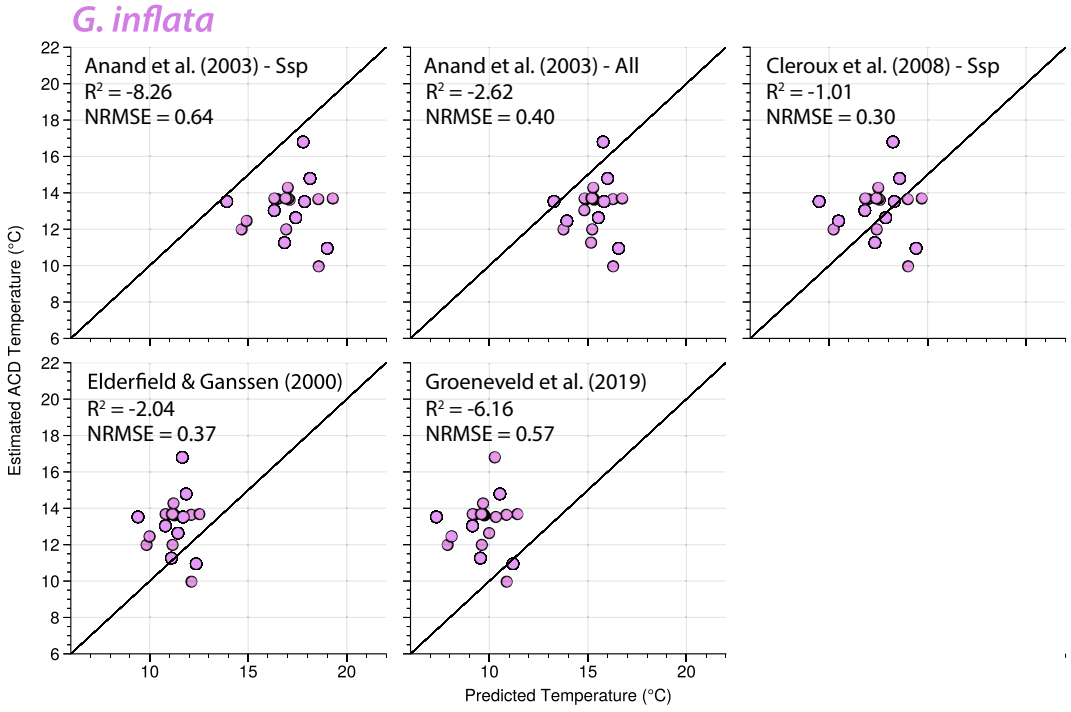

Fig. 6. Observed vs. predicted temperatures using previously published equations for *G. inflata*. Equation reference and associated fit statistics are included in the upper left corner of each subplot. A 1:1 relationship is represented by the solid black line.

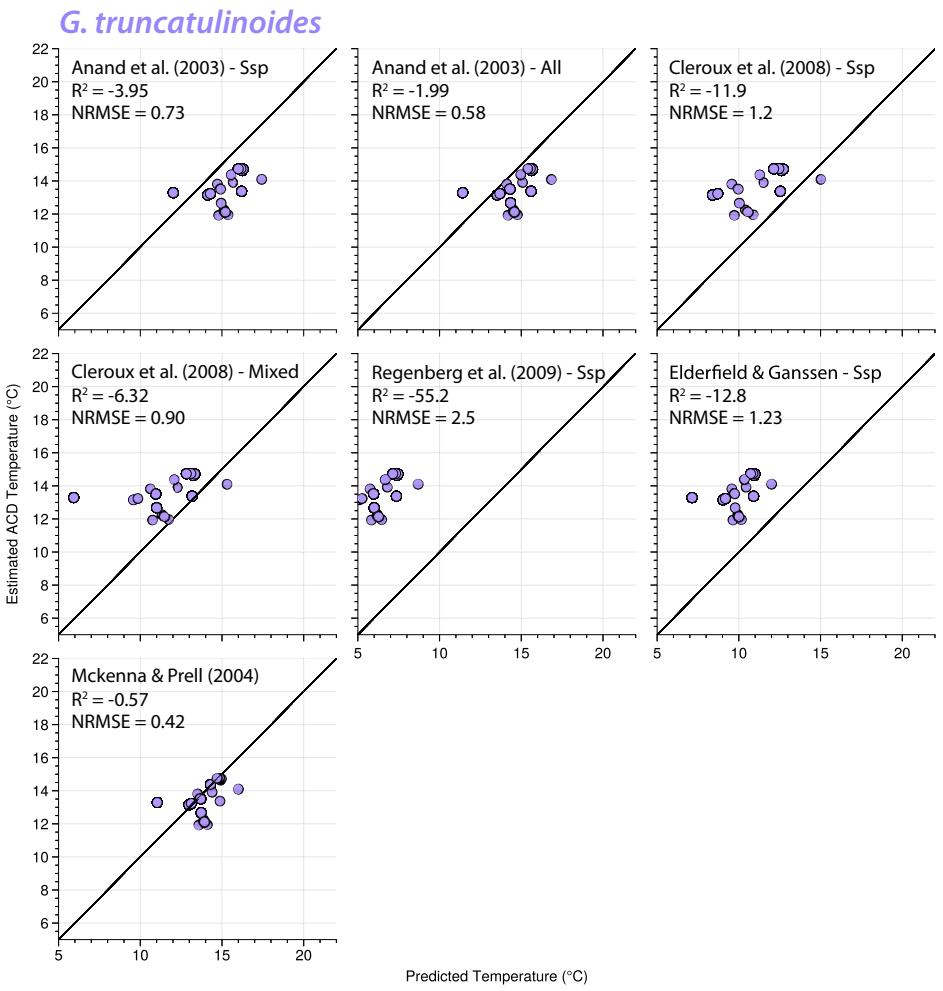

Fig. 7. Observed vs. predicted temperatures using previously published equations for *G. truncatulinoides*. Equation reference and associated fit statistics are included in the upper left corner of each subplot. A 1:1 relationship is represented by the solid black line.

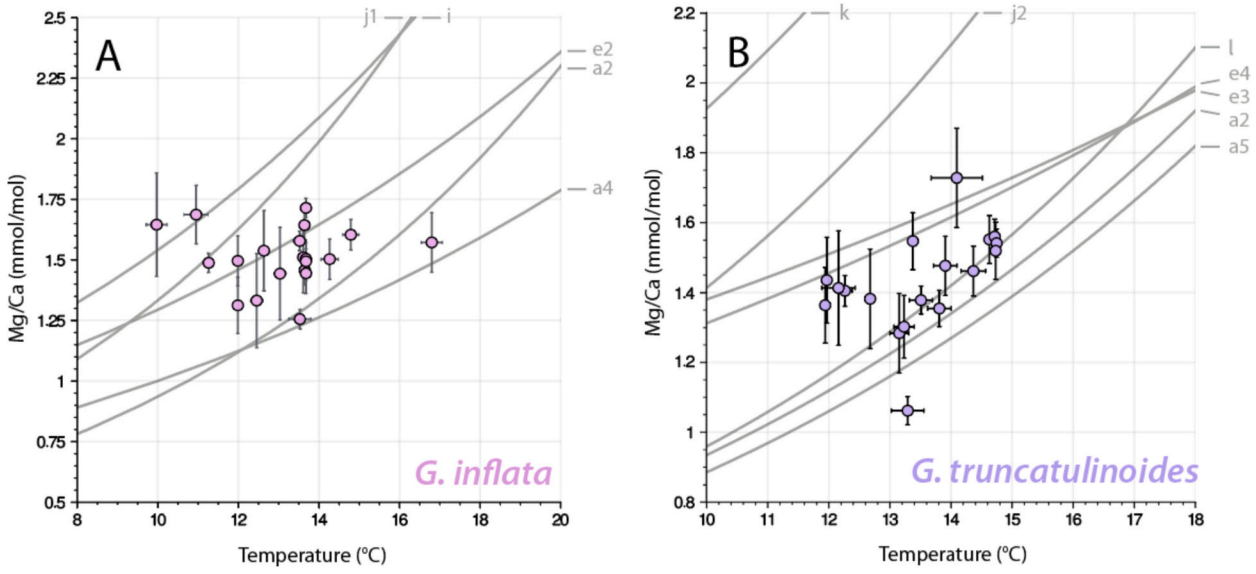

Fig. 8. Comparing the fit and performance of previously published models (gray regression lines) for (A) *G. inflata* and (B) *G. truncatulinoides*. Published regressions are denoted with letters that identify their source publication and related statistics detailed in Table 6.

For surface-dwelling *G. bulloides*, the most viable calibration model was a temperature-only regression with an apparent temperature sensitivity (7.7 ± 0.2 % per °C) that aligns with previously published calibration studies. Nominally, the "best" calibration model included a substantial negative correlation with salinity. However, these results stem from the exclusive representation of the high Mg/Ca endmember by core tops under the influence of the southeast monsoon off the Java/Sumatran coast. Rerunning our analysis on the Java/Sumatran cores and south Indian Ocean cores separately suggests that temperature-only models are the "best" empirical fit to the data, but regional collinearity between temperature and other nonthermal parameters limits our capacity to conclude that nonthermal variables have no bearing on *G. bulloides* Mg/Ca. We therefore recommend using the temperature-only regression from the full dataset for reconstructions in the area until additional data can help clarify secondary controls on *G. bulloides* Mg/Ca.

Finally, insights from subsurface-dwelling *G. inflata* and *G. truncatulinoides* data were limited largely due to the narrow range in ocean temperature and other parameters during both species' growth season in the southeast Indian Ocean. In lieu of developing our own equations, we compared the predictive skill of previously published temperature-only equations on the Indian Ocean dataset. While some yielded more accurate temperature estimates than others, ultimately the signal-to-noise ratio in the subsurface species datasets was too low to identify a clear, preferred equation to use in the region. We call for further studies like this one to add to the growing *G. inflata* and *G. truncatulinoides* database for the Indian Ocean to further constrain these relationships.

CRediT authorship contribution statement

Ryan H. Glaubke: Writing – review & editing, Validation, Formal analysis, Writing – original draft, Methodology, Data curation, Visualization, Investigation, Conceptualization. **Elisabeth L. Sikes:** Writing – review & editing, Investigation, Supervision, Funding acquisition, Project administration, Conceptualization. **Natalie E. Umling:** Writing – review & editing, Investigation, Visualization, Formal analysis, Supervision, Data curation. **Katherine A. Allen:** Writing – review & editing, Supervision, Methodology, Investigation. **Matthew W. Schmidt:** Resources, Writing – review & editing, Methodology, Supervision, Investigation.

Declaration of competing interest

The authors declare that they have no known competing financial interests or personal relationships that could have appeared to influence the work reported in this paper.

Acknowledgments

The authors wish to thank the two anonymous reviewers whose comments improved the quality of our manuscript. We are grateful to the captain, crew, and shipboard scientists aboard the R/V *Thomas G. Thompson* for their help collecting samples during the CROCCA-2S expedition (TN362). We also wish to acknowledge Jason Curtis, Bettina Sohst and Brian Giebel for their assistance with geochemical analyses. This work was supported by the National Science Foundation (Grants OCE 1559080, OCE 1940962, and OCE 2002642 awarded to E.L. S.).

Appendix A. Supplementary data

Supplementary data to this article can be found online at https://doi.org/10.1016/j.palaeo.2025.113190.

Data availability

The data used in this study can be accessed as a spreadsheet in the supporting material. The code developed for our depth habitat estimates and calibration exercises are archived as a collection of jupyter notebooks archived through Zenodo (https://doi.org/10.5281/zenodo.15627456).

References

Allen, K.A., Hönisch, B., Eggins, S.M., Haynes, L.L., Rosenthal, Y., Yu, J., 2016. Trace element proxies for surface ocean conditions: A synthesis of culture calibrations with planktic foraminifera. Geochimica et Cosmochimica Acta 193, 197–221. https://doi.org/10.1016/j.gca.2016.08.015.

Anand, P., Elderfield, H., Conte, M.H., 2003. Calibration of Mg/Ca thermometry in planktonic foraminifera from a sediment trap time series. Paleoceanography 18 (2). https://doi.org/10.1029/2002pa000846.

Arbuszewski, J., deMenocal, P., Kaplan, A., Farmer, E.C., 2010. On the fidelity of shell-derived δ18Oseawater estimates. Earth Planet. Sci. Lett. 300 (3–4), 185–196. https://doi.org/10.1016/j.epsl.2010.10.035.

Belsley, D.A., Kuh, E., Welsch, R.E., 1980. Regression Diagnostics. Wiley Series in Probability and Statistics. https://doi.org/10.1002/0471725153.

Cléroux, C., Cortijo, E., Duplessy, J., Zahn, R., 2007. Deep-dwelling foraminifera as thermocline temperature recorders. Geochem. Geophys. Geosyst. 8 (4). https://doi.org/10.1029/2006gc001474.

Cléroux, C., Cortijo, E., Anand, P., Labeyrie, L., Bassinot, F., Caillon, N., Duplessy, J., 2008. Mg/ca and Sr/ca ratios in planktonic foraminifera: Proxies for upper water column temperature reconstruction. Paleoceanography 23 (3), n/a–n/a. https://doi.org/10.1029/2007pa001505.

Cléroux, C., Lynch-Stieglitz, J., Schmidt, M.W., Cortijo, E., Duplessy, J.-C., 2009. Evidence for calcification depth change of G loborotalia truncatulinoides between deglaciation and Holocene in the Western Atlantic Ocean. Mar. Micropaleontol. 73 (1–2), 57–61. https://doi.org/10.1016/j.marmicro.2009.07.001.

Curry, W.B., Ostermann, D.R., Guptha, M.V.S., Ittekkot, V., 1992. Foraminiferal production and monsoonal upwelling in the Arabian Sea: evidence from sediment traps. Geol. Soc. Lond. Spec. Publ. 64 (1), 93–106. https://doi.org/10.1144/gsl.sp.1992.064.01.06.

Dahl, K.A., Oppo, D.W., 2006. Sea surface temperature pattern reconstructions in the Arabian Sea. Paleoceanography 21 (1). https://doi.org/10.1029/2005pa001162.

Dalal, D.K., Zickar, M.J., 2012. Some common myths about centering predictor variables in moderated multiple regression and polynomial regression. Organ. Res. Methods 15 (3), 339–362. https://doi.org/10.1177/1094428111430540.

Dekens, P.S., Lea, D.W., Pak, D.K., Spero, H.J., 2002. Core top calibration of Mg/Ca in tropical foraminifera: refining paleotemperature estimation. Geochem. Geophys. Geosyst. 3 (4), 1–29. https://doi.org/10.1029/2001gc000200.

Dueñas-Bohórquez, A., da Rocha, R.E., Kuroyanagi, A., Bijma, J., Reichart, G.-J., 2009. Effect of salinity and seawater calcite saturation state on Mg and Sr incorporation in cultured planktonic foraminifera. Mar. Micropaleontol. 73 (3–4), 178–189. https://doi.org/10.1016/j.marmicro.2009.09.002.

Durazzi, J.T., 1981. Stable-isotope studies of planktonic foraminifera in North Atlantic core tops. Palaeogeogr. Palaeoclimatol. Palaeoecol. 33 (1–3), 157–172. https://doi.org/10.1016/0031-0182(81)90036-5.

Elderfield, H., Ganssen, G., 2000. Past temperature and δ18O of surface ocean waters inferred from foraminiferal Mg/Ca ratios. Nature 405 (6785), 442–445. https://doi.org/10.1038/35013033.

Epstein, S., Mayeda, T., 1953. Variation of O18 content of waters from natural sources. Geochim. Cosmochim. Acta 4 (5), 213–224. https://doi.org/10.1016/0016-7037(53)90051-9.

Fairbanks, R.G., Wiebe, P.H., Bé, A.W.H., 1980. Vertical distribution and isotopic composition of living planktonic foraminifera in the Western North Atlantic. Science 207 (4426), 61–63. https://doi.org/10.1126/science.207.4426.61.

Evans, D., Wade, B.S., Henehan, M., Erez, J., Müller, W., 2016. Revisiting carbonate chemistry controls on planktic foraminifera Mg/Ca: implications for sea surface temperature and hydrology shifts over the Paleocene-Eocene Thermal Maximum and Eocene-Oligocene transition. Climate of the Past 12 (4), 819–835. https://doi.org/10.5194/cp-12-819-2016.

Fairbanks, R.G., Sverdlove, M., Free, R., Wiebe, P.H., Bé, A.W.H., 1982. Vertical distribution and isotopic fractionation of living planktonic foraminifera from the Panama Basin. Nature 298 (5877), 841–844. https://doi.org/10.1038/298841a0.

Farmer, E.C., Kaplan, A., de Menocal, P.B., Lynch-Stieglitz, J., 2007. Corroborating ecological depth preferences of planktonic foraminifera in the tropical Atlantic with the stable oxygen isotope ratios of core top specimens. Paleoceanography 22 (3). https://doi.org/10.1029/2006pa001361.

Ferguson, J.E., Henderson, G.M., Kucera, M., Rickaby, R.E.M., 2008. Systematic change of foraminiferal Mg/Ca ratios across a strong salinity gradient. Earth Planet. Sci. Lett. 265 (1–2), 153–166. https://doi.org/10.1016/j.epsl.2007.10.011.

Glaubke, R.H., Sikes, E.L., Sosdian, S.M., Umling, N.E., Starr, A., Moffa-Sanchez, P.L., Schmidt, M.W., 2025. Elevated shallow water salinity in the deglacial Indian Ocean was sourced from the deep. Nature Geoscience 1–8. https://doi.org/10.1038/s41561-025-01756-7.

Glaubke, R.H., Wagner, A.J., Sikes, E.L., 2024. Characterizing the stable oxygen isotopic composition of the Southeast Indian Ocean. Mar. Chem. 262, 104397. https://doi.org/10.1016/j.marchem.2024.104397.

Gray, W.R., Evans, D., 2019. Nonthermal Influences on Mg/Ca in planktonic foraminifera: A review of culture studies and application to the last glacial maximum. Paleoceanogr. Paleoclimatol. 34 (3), 306–315. https://doi.org/10.1029/2018pa003517.

Gray, W.R., Weldeab, S., Lea, D.W., Rosenthal, Y., Gruber, N., Donner, B., Fischer, G., 2018. The effects of temperature, salinity, and the carbonate system on Mg/Ca in Globigerinoides ruber (white): A global sediment trap calibration. Earth Planet. Sci. Lett. 482, 607–620. https://doi.org/10.1016/j.epsl.2017.11.026.

Groeneveld, J., Chiessi, C.M., 2011. Mg/ca of *Globorotalia inflata* as a recorder of permanent thermocline temperatures in the South Atlantic. Paleoceanography 26 (2). https://doi.org/10.1029/2010pa001940.

Groeneveld, J., Ho, S.L., Mackensen, A., Mohtadi, M., Laepple, T., 2019. Deciphering the variability in Mg/Ca and stable oxygen isotopes of individual foraminifera. Paleoceanogr. Paleoclimatol. 34 (5), 755–773. https://doi.org/10.1029/2018pa003533.

Heaton, T.J., Köhler, P., Butzin, M., Bard, E., Reimer, R.W., Austin, W.E.N., Ramsey, C.B., Grootes, P.M., Hughen, K.A., Kromer, B., Reimer, P.J., Adkins, J., Burke, A., Cook, M. S., Olsen, J., Skinner, L.C., 2020. Marine20—the marine radiocarbon age calibration curve (0–55,000 cal BP). Radiocarbon 62 (4), 779–820. https://doi.org/10.1017/rdc.2020.68.

Hemleben, C., Spindler, M., Breitinger, I., Deuser, W.G., 1985. Field and laboratory studies on the ontogeny and ecology of some globorotaliid species from the Sargasso Sea off Bermuda. J. Foraminifer. Res. 15 (4), 254–272. https://doi.org/10.2113/gsjfr.15.4.254.

Hertzberg, J.E., Schmidt, M.W., 2013. Refining Globigerinoides ruber Mg/Ca paleothermometry in the Atlantic Ocean. Earth Planet. Sci. Lett. 383, 123–133. https://doi.org/10.1016/j.epsl.2013.09.044.

Holland, K., Branson, O., Haynes, L.L., Hönisch, B., Allen, K.A., Russell, A.D., et al., 2020. Constraining multiple controls on planktic foraminifera Mg/Ca. Geochim. Cosmochim. Acta 273, 116–136. https://doi.org/10.1016/j.gca.2020.01.015.

Hollstein, M., Mohtadi, M., Rosenthal, Y., Sanchez, P.M., Oppo, D., Méndez, G.M., et al., 2017. Stable oxygen isotopes and Mg/Ca in planktic foraminifera from modern surface sediments of the Western Pacific warm pool: implications for thermocline reconstructions. Paleoceanography 32 (11), 1174–1194. https://doi.org/10.1002/2017pa003122.

Hönisch, B., Allen, K.A., Lea, D.W., Spero, H.J., Eggins, S.M., Arbuszewski, J., et al., 2013. The influence of salinity on Mg/Ca in planktic foraminifers – evidence from cultures, core-top sediments and complementary δ18O. Geochim. Cosmochim. Acta 121, 196–213. https://doi.org/10.1016/j.gca.2013.07.028.

Hoogakker, B.A.A., Klinkhammer, G.P., Elderfield, H., Rohling, E.J., Hayward, C., 2009. Mg/Ca paleothermometry in high salinity environments. Earth Planet. Sci. Lett. 284 (3–4), 583–589. https://doi.org/10.1016/j.epsl.2009.05.027.

Humphreys, M.P., Lewis, E.R., Sharp, J.D., Pierrot, D., 2021. PyCO2SYS v1.8: marine carbonate system calculations in Python. Geosci. Model Dev. 15 (1), 15–43. https://doi.org/10.5194/gmd-15-15-2022.

Jefferys, W.H., Berger, J.O., 1992. Ockham's razor and Bayesian analysis. Am. Sci. 80 (1), 64–72. http://www.jstor.org/stable/29774559.

Johnson, V.E., Pramanik, S., Shudde, R., 2023. Bayes factor functions for reporting outcomes of hypothesis tests. Proc. Natl. Acad. Sci. USA 120 (8), e2217331120. https://doi.org/10.1073/pnas.2217331120.

Jonkers, L., Kučera, M., 2015. Global analysis of seasonality in the shell flux of extant planktonic Foraminifera. Biogeosciences 12 (7), 2207–2226. https://doi.org/10.5194/bg-12-2207-2015.

Jonkers, L., Gopalakrishnan, A., Weßel, L., Chiessi, C.M., Groeneveld, J., Monien, P., et al., 2021. Morphotype and Crust Effects on the Geochemistry of Globorotalia inflata. Paleoceanogr. Paleoclimatol. 36 (4). https://doi.org/10.1029/2021pa004224.

Kass, R.E., Raftery, A.E., 2012. Bayes factors. J. Am. Stat. Assoc. 90 (430), 773–795. https://doi.org/10.1080/01621459.1995.10476572.

Khider, D., Huerta, G., Jackson, C., Stott, L.D., Emile-Geay, J., 2015. A Bayesian, multivariate calibration for Globigerinoides ruber Mg/ca. Geochem. Geophys. Geosyst. 16 (9), 2916–2932. https://doi.org/10.1002/2015gc005844.

King, A.L., Howard, W.R., 2001. Seasonality of foraminiferal flux in sediment traps at Chatham Rise, SW Pacific: implications for paleotemperature estimates. Deep-Sea Res. I Oceanogr. Res. Pap. 48 (7), 1687–1708. https://doi.org/10.1016/s0967-0637(00)00106-0.

King, A.L., Howard, W.R., 2005. δ18O seasonality of planktonic foraminifera from Southern Ocean sediment traps: Latitudinal gradients and implications for paleoclimate reconstructions. Mar. Micropaleontol. 56 (1–2), 1–24. https://doi.org/10.1016/j.marmicro.2005.02.008.

Kısakürek, B., Eisenhauer, A., Böhm, F., Garbe-Schönberg, D., Erez, J., 2008. Controls on shell Mg/Ca and Sr/Ca in cultured planktonic foraminiferan, Globigerinoides ruber (white). Earth Planet. Sci. Lett. 273 (3–4), 260–269. https://doi.org/10.1016/j.epsl.2008.06.026.

Koch-Larrouy, A., Morrow, R., Penduff, T., Juza, M., 2010. Origin and mechanism of Subantarctic Mode Water formation and transformation in the Southern Indian Ocean. Ocean Dyn. 60 (3), 563–583. https://doi.org/10.1007/s10236-010-0276-4.

Koziol, A.M., Newton, R.C., 1995. Experimental determination of the reactions magnesite + quartz = enstatite + CO2 and magnesite = periclase + CO2, and enthalpies of formation of enstatite and magnesite. Am. Mineral. 80 (11−12), 1252–1260. https://doi.org/10.2138/am-1995-11-1215.

Kuroyanagi, A., Kawahata, H., 2004. Vertical distribution of living planktonic foraminifera in the seas around Japan. Mar. Micropaleontol. 53 (1–2), 173–196. https://doi.org/10.1016/j.marmicro.2004.06.001.

Lauvset, S.K., Key, R.M., Olsen, A., van Heuven, S., Velo, A., Lin, X., et al., 2016. A new global interior ocean mapped climatology: the 1∘ × 1∘ GLODAP version 2. Earth Syst. Sci. Data 8 (2), 325–340. https://doi.org/10.5194/essd-8-325-2016.

Lea, D.W., 2014. Elemental and isotopic proxies of past ocean temperatures. In: Holland, H.D., Turekian, K.K. (Eds.), Treatise on Geochemistry (Second Edition), 8, pp. 373–397. https://doi.org/10.1016/b978-0-08-095975-7.00614-8.

Lea, D.W., Mashiotta, T.A., Spero, H.J., 1999. Controls on magnesium and strontium uptake in planktonic foraminifera determined by live culturing. Geochim. Cosmochim. Acta 63 (16), 2369–2379. https://doi.org/10.1016/s0016-7037(99)00197-0.

Lea, D.W., Pak, D.K., Spero, H.J., 2000. Climate impact of late quaternary equatorial pacific sea surface temperature variations. Science 289 (5485), 1719–1724. https://doi.org/10.1126/science.289.5485.1719.

Lebigot, E.O., 2022. Uncertainties: a Python package for calculations with uncertainties (Version 3.1.7). http://pythonhosted.org/uncertainties/.

Lee, M.D., Wagenmakers, E.-J., 2014. Bayesian Cognitive Modeling: A Practical Course. Cambridge University Press. https://doi.org/10.1017/cbo9781139087759.

LeGrande, A.N., Schmidt, G.A., 2006. Global gridded data set of the oxygen isotopic composition in seawater. Geophys. Res. Lett. 33 (12). https://doi.org/10.1029/2006gl026011.

LeGrande, A.N., Lynch-Stieglitz, J., Farmer, E.C., 2004. Oxygen isotopic composition of *Globorotalia truncatulinoides* as a proxy for intermediate depth density. Paleoceanography 19 (4). https://doi.org/10.1029/2004pa001045.

Marr, J.P., Baker, J.A., Carter, L., Allan, A.S.R., Dunbar, G.B., Bostock, H.C., 2011. Ecological and temperature controls on Mg/ca ratios of *Globigerina bulloides* from the Southwest Pacific Ocean. Paleoceanography 26 (2). https://doi.org/10.1029/2010pa002059.

McKenna, V.S., Prell, W.L., 2004. Calibration of the Mg/ca of *Globorotalia truncatulinoides* (R) for the reconstruction of marine temperature gradients. Paleoceanography 19 (2). https://doi.org/10.1029/2000pa000604.

Miles, J., Shevlin, M., 2001. Applying Regression and Correlation: A Guide for Students and Researchers. Sage.

Mohtadi, M., Steinke, S., Groeneveld, J., Fink, H.G., Rixen, T., Hebbeln, D., et al., 2009. Low-latitude control on seasonal and interannual changes in planktonic foraminiferal flux and shell geochemistry off South Java: a sediment trap study. Paleoceanography 24 (1). https://doi.org/10.1029/2008pa001636.

Mohtadi, M., Oppo, D.W., Lückge, A., DePol-Holz, R., Steinke, S., Groeneveld, J., et al., 2011. Reconstructing the thermal structure of the upper ocean: insights from planktic foraminifera shell chemistry and alkenones in modern sediments of the tropical eastern Indian Ocean. Paleoceanography 26 (3). https://doi.org/10.1029/2011pa002132.

Mortyn, P.G., Charles, C.D., 2003. Planktonic foraminiferal depth habitat and δ18O calibrations: Plankton tow results from the Atlantic sector of the Southern Ocean. Paleoceanography 18 (2). https://doi.org/10.1029/2001pa000637.

Mulitza, S., Dürkoop, A., Hale, W., Wefer, G., Niebler, H.S., 1997. Planktonic foraminifera as recorders of past surface-water stratification. Geology 25 (4), 335–338. https://doi.org/10.1130/0091-7613(1997)025<0335:pfarop>2.3.co;2.

Navrotsky, A., Capobianco, C., 1987. Enthalpies of formation of dolomite and of magnesian calcites. Am. Mineral. 72 (7–8), 782–787.

Northcote, L.C., Neil, H.L., 2005. Seasonal variations in foraminiferal flux in the Southern Ocean, Campbell Plateau, New Zealand. Mar. Micropaleontol. 56 (3–4), 122–137. https://doi.org/10.1016/j.marmicro.2005.05.001.

Nürnberg, D., Bijma, J., Hemleben, C., 1996. Assessing the reliability of magnesium in foraminiferal calcite as a proxy for water mass temperatures. Geochim. Cosmochim. Acta 60 (5), 803–814. https://doi.org/10.1016/0016-7037(95)00446-7.

O'brien, R.M., 2007. A caution regarding rules of thumb for variance inflation factors. Qual. Quant. 41 (5), 673–690. https://doi.org/10.1007/s11135-006-9018-6.

Oomori, T., Kaneshima, H., Maezato, Y., Kitano, Y., 1987. Distribution coefficient of Mg2 + ions between calcite and solution at 10–50°C. Mar. Chem. 20 (4), 327–336. https://doi.org/10.1016/0304-4203(87)90066-1.

Peeters, F.J.C., Brummer, G.-J.A., 2002. The seasonal and vertical distribution of living planktic foraminifera in the NW Arabian Sea. Geol. Soc. Lond. Spec. Publ. 195 (1), 463–497. https://doi.org/10.1144/gsl.sp.2002.195.01.26.

Pelejero, C., Calvo, E., McCulloch, M.T., Marshall, J.F., Gagan, M.K., Lough, J.M., Opdyke, B.N., 2005. Preindustrial to modern interdecadal variability in coral reef pH. Science 309 (5744), 2204–2207. https://doi.org/10.1126/science.1113692.

Ravelo, A.C., Fairbanks, R.G., 1992. Oxygen isotopic composition of multiple species of planktonic foraminifera: recorders of the modern photic zone temperature gradient. Paleoceanography 7 (6), 815–831. https://doi.org/10.1029/92pa02092.

Rebotim, A., Voelker, A.H.L., Jonkers, L., Waniek, J.J., Meggers, H., Schiebel, R., et al., 2017. Factors controlling the depth habitat of planktonic foraminifera in the subtropical eastern North Atlantic. Biogeosciences 14 (4), 827–859. https://doi.org/10.5194/bg-14-827-2017.

Rebotim, A., Voelker, A.H.L., Jonkers, L., Waniek, J.J., Schulz, M., Kucera, M., 2019. Calcification depth of deep-dwelling planktonic foraminifera from the eastern North Atlantic constrained by stable oxygen isotope ratios of shells from stratified plankton tows. J. Micropalaeontol. 38 (2), 113–131. https://doi.org/10.5194/jm-38-113-2019.

Regenberg, M., Regenberg, A., Garbe-Schönberg, D., Lea, D.W., 2014. Global dissolution effects on planktonic foraminiferal Mg/Ca ratios controlled by the calcite-saturation state of bottom waters. Paleoceanography 29 (3), 127–142. https://doi.org/10.1002/2013pa002492.

Regenberg, M., Steph, S., Nürnberg, D., Tiedemann, R., Garbe-Schönberg, D., 2009. Calibrating Mg/ca ratios of multiple planktonic foraminiferal species with δ 18O-calcification temperatures: paleothermometry for the upper water column. Earth Planet. Sci. Lett. 278 (3–4), 324–336. https://doi.org/10.1016/j.epsl.2008.12.019.

Reynolds, C.E., Richey, J.N., Fehrenbacher, J.S., Rosenheim, B.E., Spero, H.J., 2018. Environmental controls on the geochemistry of Globorotalia truncatulinoides in the Gulf of Mexico: Implications for paleoceanographic reconstructions. Mar. Micropaleontol. 142, 92–104. https://doi.org/10.1016/j.marmicro.2018.05.006.

Riveiros, N.V., Govin, A., Waelbroeck, C., Mackensen, A., Michel, E., Moreira, S., et al., 2016. Mg/ca thermometry in planktic foraminifera: improving paleotemperature estimations for G. bulloides and N. pachyderma left. Geochem. Geophys. Geosyst. 17 (4), 1249–1264. https://doi.org/10.1002/2015gc006234.

Romero, E., Tenorio-Fernandez, L., Portela, E., Montes-Aréchiga, J., Sánchez-Velasco, L., 2023. Improving the thermocline calculation over the global ocean. Ocean Sci. 19 (3), 887–901. https://doi.org/10.5194/os-19-887-2023.

Rosenthal, Y., Lohmann, G.P., Lohmann, K.C., Sherrell, R.M., 2000. Incorporation and preservation of Mg in Globigerinoides sacculifer: implications for reconstructing the temperature and 18O/16O of seawater. Paleoceanography 15 (1), 135–145. https://doi.org/10.1029/1999pa000415.

Rouder, J.N., Morey, R.D., Province, J.M., 2013. A Bayes factor meta-analysis of recent extrasensory perception experiments: comment on storm, Tressoldi, and Di Risio (2010). Psychol. Bull. 139 (1), 241–247. https://doi.org/10.1037/a0029008.

Russell, A.D., Hönisch, B., Spero, H.J., Lea, D.W., 2004. Effects of seawater carbonate ion concentration and temperature on shell U, Mg, and Sr in cultured planktonic foraminifera. Geochim. Cosmochim. Acta 68 (21), 4347–4361. https://doi.org/10.1016/j.gca.2004.03.013.

Sadekov, A., Eggins, S.M., Deckker, P.D., Kroon, D., 2008. Uncertainties in seawater thermometry deriving from intratest and intertest Mg/Ca variability in Globigerinoides ruber. Paleoceanography 23 (1). https://doi.org/10.1029/2007pa001452.

Saenger, C.P., Evans, M.N., 2019. Calibration and validation of environmental controls on planktic foraminifera Mg/Ca using global core-top data. Paleoceanogr. Paleoclimatol. 34 (8), 1249–1270. https://doi.org/10.1029/2018pa003507.

Sallée, J.-B., Wienders, N., Speer, K., Morrow, R., 2006. Formation of subantarctic mode water in the southeastern Indian Ocean. Ocean Dyn. 56 (5–6), 525–542. https://doi.org/10.1007/s10236-005-0054-x.

Salmon, K.H., Anand, P., Sexton, P.F., Conte, M., 2016. Calcification and growth processes in planktonic foraminifera complicate the use of B/ca and U/ca as carbonate chemistry proxies. Earth Planet. Sci. Lett. 449 (Glob. Biogeochem. Cycles 10 1996), 372–381. https://doi.org/10.1016/j.epsl.2016.05.016.

Sautter, L.R., Thunell, R.C., 1991. Seasonal variability in the δ18O and δ13C of planktonic foraminifera from an upwelling environment: sediment trap results from the San Pedro Basin, Southern California Bight. Paleoceanography 6 (3), 307–334. https://doi.org/10.1029/91pa00385.

Schiebel, R., Hemleben, C., 2017. Planktic Foraminifers in the Modern Ocean (second). Springer. https://doi.org/10.1007/978-3-662-50297-6.

Schiebel, R., Spielhagen, R.F., Garnier, J., Hagemann, J., Howa, H., Jentzen, A., et al., 2017. Modern planktic foraminifers in the high-latitude ocean. Mar. Micropaleontol. 136, 1–13. https://doi.org/10.1016/j.marmicro.2017.08.004.

Schmitt, A., Elliot, M., Thirumalai, K., La, C., Bassinot, F., Petersen, J., et al., 2019. Single foraminifera Mg/Ca analyses of past glacial-interglacial temperatures derived from G. ruber sensu stricto and sensu lato morphotypes. Chem. Geol. 511, 510–520. https://doi.org/10.1016/j.chemgeo.2018.11.007.

Shackleton, N.J., 1974. Attainment of Isotopic Equilibrium between Ocean Water and the Benthonic Foraminifera Genus Uvigerina: Isotopic Changes in the Ocean during the Last Glacial. Colloques Internationaux Du CNRS.

Spero, H.J., Mielke, K.M., Kalve, E.M., Lea, D.W., Pak, D.K., 2003. Multispecies approach to reconstructing eastern equatorial Pacific thermocline hydrography during the past 360 kyr. Paleoceanography 18 (1). https://doi.org/10.1029/2002pa000814.

Tierney, J.E., Malevich, S.B., Gray, W., Vetter, L., Thirumalai, K., 2019. Bayesian Calibration of the Mg/Ca Paleothermometer in Planktic Foraminifera. Paleoceanogr. Paleoclimatol. 34 (12), 2005–2030. https://doi.org/10.1029/2019pa003744.

Wang, L., 2000. Isotopic signals in two morphotypes of *Globigerinoides ruber* (white) from the South China Sea: implications for monsoon climate change during the last glacial cycle. Palaeogeogr. Palaeoclimatol. Palaeoecol. 161 (3–4), 381–394. https://doi.org/10.1016/s0031-0182(00)00094-8.

Williams, D.F., Healy-Williams, N., 1980. Oxygen isotopic-hydrographic relationships among recent planktonic Foraminifera from the Indian Ocean. Nature 283 (5750), 848–852. https://doi.org/10.1038/283848a0.